Title

New physical insights into the supporting subspace factorization of XMS-CASPT2 and generalization to multiple spin states via spin-free formulation

Journal

The Journal of Chemical Physics, 160(12)

ISSN

0021-9606

Author

Song, Chenchen

Publication Date

2024-03-28

DOI

10.1063/5.0192478

New physical insights into the supporting subspace factorization of XMS-CASPT2 and generalization to multiple spin states via spin-free formulation

Chenchen Song[1, a)]

Department of Chemistry, University of California Davis, 1 Shields Ave, Davis, CA 95616, USA.

This paper introduces a spin-free formulation of the supporting subspace factorization (J.Chem.Phys, 149, 044108 (2018)), enabling a reduction in the computational scaling of extended multi-state complete active space second-order perturbation method (XMS-CASPT2) for arbitrary spins. Compared to the original formulation that is defined in the spin orbitals and is limited to singlet states, the spin-free formulation in this work treats different spin states equivalently, thus naturally generalizes the idea beyond singlet states. In addition, we will present a new way of deriving the supporting subspace factorization with the purpose of understanding its physical interpretation. In this new derivation, we separate the sources that make CASPT2 difficult into the "same-site interactions" and "inter-site interactions". We will first show how the Kronecker sum can be used to remove the same-site interactions in the absence of inter-site interactions, leading to MP2 energy in dressed orbitals. We will then show how the inter-site interactions can be exactly recovered using Löwdin partition, where the supporting subspace concept will naturally arise. The new spin-free formulation maintains the main advantage of the supporting subspace factorization, i.e. allowing XMS-CASPT2 energies to be computed using highly optimized MP2 energy codes and Fock build codes, thus reducing the scaling of XMS-CASPT2 to the same scaling as MP2. We will present and discuss results that benchmark the accuracy and performance of the new method. To demonstrate how the new method can be useful in studying real photochemical systems, the supporting subspace XMS-CASPT2 is applied to a photoreaction sensitive to magnetic field effects. The new spin-free formulation makes it possible to calculate the doublet and quartet states required in this particular photoreaction mechanism.

[a)]Electronic mail: ccsong@ucdavis.edu

I. INTRODUCTION

Photophysical and photochemical processes often involve excited states of different spins. For example, intersystem crossing between singlet and triplet states plays an important role in generating reactive oxygen species in photodynamic therapy.[1,2] Another example is the time-resolved photo-electron spectroscopy for organic molecules, where information about the singlet or triplet excited states and the doublet ionized state are both needed to interpret the experimental signals.[3,4] In addition, molecules that exhibit notable spin-dependent photoreactivity are found to be susceptible to magnetic field effects,[5] which is hypothesized to play a role in the magnetoreception of birds and plants.[6,7] Theoretical studies of these photochemical processes require consistent treatments of different spin states.

One of the most widely used theoretical methods for studying photochemistry is the complete active space second order perturbation theory (CASPT2).[8,9] The method captures static electron correlation using reference obtained from complete active space self consistent field calculations (CASSCF),[10–12] and captures dynamic electron correlation through second order perturbation theory.[13] Since it was first proposed,[14–16] much progress has been made to further improve the method and address some of its limitations, a few examples of which are summarized here. One common issue of CASPT2 is the intruder-state problem, which may arise if a state in the first-order interacting space is near-degenerate with the reference state. A common way to remedy this problem is through regularization, such as the simple level-shift technique[17,18] or the more rigorous σ^p-regularization.[19] The use of the spin-averaged Fock operator as the zeroth order Hamiltonian in CASPT2 is known to give an imbalanced treatment between the open shell and closed shell configurations,[8,20] and different modifications to the zeroth order Hamiltonian operator[18,21–23] have been proposed to address this issue. To address the behavior that spurious crossings can occur in state-specific CASPT2 potential energy curves, multi-state CASPT2[24] has been developed based on quasi-degenerate preturbation theory using reference space spanned by multiple wavefunctions. This is further improved by the extended multi state CASPT2 (XMS-CASPT2),[25] which ensures invariance with respect to unitary rotations within the reference space. However, XMS-CASPT2 energies can be sensitive to inclusion of additional electronic states even when the added states are much higher in energy, and this drawback is further addressed with the introduction of

the dynamic weighted scheme.[26] Analytical gradients[27,28] and non-adiabatic couplings[29] have also been developed for many of the aforementioned methods. As a result of all these developments, CASPT2 has become one of the most reliable methods for studying photochemical processes.

Applications of CASPT2 to large molecular systems are often limited by its steep computational scaling, which increases as $O(N^6)$ with the number of atomic orbitals for a chosen active space setting. Similar to other correlation methods, the high scaling of CASPT2 arises from the high order tensors present in the working equations, such as the fourth order electron repulson integral (ERI) tensors, energy denominators arising from the resolvent operator, and the wavefunction amplitudes. Tensor factorization addresses such computational bottleneck by factorizing the high order tensors into products of lower order ones in either exact or approximate ways. There have been extensive studies on tensor factorizations of ERIs, and a few such examples include resolution of identity,[30–32] pseudo-spectral,[33–35] Cholesky decomposition,[36–38] and tensor hyper-contraction (THC).[39–41] In terms of the energy denominators such as those appearing in the single reference Moller Plesset second order perturbation theory (MP2), factorization based on the Laplace transformation[42,43] is often used in the context of single reference correlation methods. The combination of THC and Laplace transformation can reduce the formal computational scaling of MP2 to $O(N^4)$ as a function of the system sizes,[39,44] which demonstrates the effectiveness of tensor factorization approaches.

Tensor factorization for wavefunction amplitudes are more complicated. In the specific case of CASPT2, one need to consider both the zeroth order and the first order wavefunction. The systems that we are aiming at in this work are photoreactions of organic molecules in complex environment involving the lowest few excited states. For such applications, a small active space (~10 active orbitals) is often sufficient to capture the multi-reference characteristics, but a large number of closed or virtual orbitals are needed for the environmental effects. As a result, the zeroth order wavefunction is seldom the bottleneck in these systems, although it is worth mentioning that when larger active spaces are required, zeroth order wavefunction can be factorized in the form of matrix products and tensor networks,[45,46] as often used in the density matrix renormalization group (DMRG) method.[47,48] The focus of this work is the first order wavefunction corresponding to the double excitation ampli-

tudes. In the context of coupled-cluster theory, there have been efforts trying to factorize the double excitation amplitudes in similar ways as the ERIs due to their similar fourth-order structure.[49,50] However, such ideas cannot be directly applied to the double excitations in CASPT2, because the multi-reference effects cause the double excitations on top of internally contracted reference to become linearly dependent, thus losing their resemblance to the ERIs.

The supporting subspace factorization[51–53] that we proposed previously provides an effective way to factorize the CASPT2 first order wavefunction using lower order tensors. When further combined with tensor factorized ERIs (e.g. tensor hyper-contraction) and the Laplace transformation of energy denominators, it reduces the scaling of CASPT2 to $O(N^4)$ with system sizes and has enabled computing excited state properties of systems with a few hundred atoms.[52] However, there were several limitations in the original formulation. The major limitation stems from the usage of spin-orbital formulation, which was chosen due to its simpler expressions. However, this requires the alpha and beta electrons to be treated separately, and the original implementation was limited to only singlet states where alpha and beta electrons can be considered as equivalent. Furthermore, the original paper[51] took a purely mathematical perspective and merely introduced the supporting subspace factorization as a mathematical trick to solve the Bloch equation. As a result, it is unclear what the introduced quantities physically represent from the original derivations.

Motivated by the limitation of the original spin orbital formulation of the supporting subspace factorization and the need to describe different spin states in photochemistry, we have developed the supporting subspace factorization based on a spin-free formulation, which is the subject of this paper. The spin-free formulation is a commonly used approach when relativistic effects are neglected and the operators involved all transform as singlet spinors.[54–56] In the context of CASPT2, the spin-free formulation is directly related to the fact that the first order interacting space is spanned only by singlet-adapted double excitations on the reference space.[57] In addition, we will also investigate the physical interpretations of supporting subspace factorization through a derivation path different from the original paper. The spin-free formulation of supporting subspace factorization will allow CASPT2 wavefunctions from different spin states to be factorized in similar ways, such that we can maintain its benefits in scaling reduction and further generalize its capability beyond only singlet states.

This paper is organized as follows. In Section II A, we start with a brief review of XMS-CASPT2 theory, in particular the Bloch equation and the spin-free formulation. In Section II B, we will discuss what contribute to the complexity of CASPT2 Bloch equation compared to when single-reference is used, which will lead to the definitions of the "same-site interactions" and the "inter-site interactions". We will then discuss how to treat these two types of interactions. In Section II C, we will first consider how the same-site interactions can be removed through Kronecker sum if the inter-site interactions are absent. In Section II D, we will then discuss how the inter-site interactions can be exactly recovered through the Löwdin partion, where the spin-free supporting subspace factorization will naturally arise. Finally, benchmark results that test the accuracy and performance of the new method as well as application to an organic photoreaction sensitive to magnetic field will be presented and discussed in Section III. To highlight the difference between the spin-free formulation in this work from the previous spin orbital formulation, we will use "the original paper" to refer to our previous work[51] where supporting subspace factorization was first proposed.

II. METHOD

A. Brief-review of XMS-CASPT2

We start with a brief review of XMS-CASPT2 theory. In this work, the zeroth order reference space is spanned by wavefunctions from SA-CASSCF calculations (denoted as $|\Phi_I\rangle$). Denote the corresponding projection operator as $\hat{P}_0 = \sum_I |\Phi_I\rangle\langle\Phi_I|$, $\hat{P}_0 + \hat{Q}_0 = 1$ and denote the corresponding Fock operator as $\hat{F}$, the zeroth order Hamiltonian is defined as

$$\hat{H}_0 = \hat{P}_0 \hat{F} \hat{P}_0 + \hat{Q}_0 \hat{F} \hat{Q}_0 \tag{1}$$

In the semi-canonical molecular orbitals, $\hat{F}$ takes the form of

$$\hat{F} = \sum_r \epsilon_r \hat{E}_{rr} + \sum_{iU} f_{iU} \left(\hat{E}_{iU} + \hat{E}_{Ui} \right) + \sum_{aU} f_{aU} \left(\hat{E}_{aU} + \hat{E}_{Ua} \right) \tag{2}$$

$$\hat{E}_{rs} = \hat{a}^\dagger_{r\alpha} \hat{a}_{s\alpha} + \hat{a}^\dagger_{r\beta} \hat{a}_{s\beta} \tag{3}$$

In the above equation, r, s denotes arbitrary molecular orbitals, while i, U, a denote closed, active and virtual orbitals respectively. In addition, the zeroth order wavefunctions are unitarily transformed such that H_0 is diagonal in the reference space, and the rotated wavefunctions will be denoted as $|\tilde{\Phi}_I\rangle$.

The XMS-CASPT2 energies are obtained from diagonalizing the effective Hamiltonian matrix $\mathbf{H}^{\text{eff}}$, and this work is based on the "single-state/single-reference" (SS-SR) contraction scheme. Although SS-SR is not fully invariant with respect to unitary rotations in the reference space, it has the benefit that computational cost only increases linearly as the number of states requested. This involves solving the state-specific Bloch equation

$$\sum_m \langle \chi_n^{(I)} | \hat{H}_0 - E_0^{(I)} + \epsilon_{\text{shift}} | \chi_m^{(I)} \rangle t_m^{(I)} = -\langle \tilde{\Phi}_I | \hat{H} | \chi_n^{(I)} \rangle \tag{4}$$

In the above equation, $t_m^{(I)}$ are the first order wavefunction amplitudes being solved for. $|\chi_n^{(I)}\rangle$ are the basis functions that span the first order interacting space, E_0 is the zeroth order energy and ϵ_{shift} is the level shift parameter. The diagonal elements of $\mathbf{H}^{\text{eff}}$ are computed as

$$H_{II}^{\text{eff}} = \langle \tilde{\Phi}_I | \hat{H} | \tilde{\Phi}_I \rangle + \sum_n \langle \tilde{\Phi}_I | \hat{H} | \chi_n^{(I)} \rangle \cdot t_n^{(I)} - \epsilon_{\text{shift}} \sum_n t_n^{(I)} \cdot t_n^{(I)} \tag{5}$$

and the off-diagonal elements are computed as

$$H_{IJ}^{\text{eff}} = \langle \tilde{\Phi}_I | \hat{H} | \tilde{\Phi}_J \rangle + \sum_n \langle \tilde{\Phi}_I | \hat{H} | \chi_n^{(J)} \rangle \cdot t_n^{(J)} \tag{6}$$

The matrix $\mathbf{H}^{\text{eff}}$ is symmetrized,[58] and then gets diagonalized to provide the XMS-CASPT2 energies. The bottleneck for XMS-CASPT2 calculations is solving the state-specific Bloch equation Eq.4 that leads to the diagonal elements, while the off-diagonal elements can be easily computed from dot product once the amplitudes are available. Therefore, in the following discussions, we will focus on how to solve Eq.4 efficiently to get the diagonal elements in Eq.5. These discussions can be easily applied to the off-diagonal elements due to the close resemblance between Eq.5 and Eq.6.

B. Types of interactions in the Spin-free Bloch equation

To keep the notations simple, during the discussions about the state specific Bloch equation Eq.4, we will drop the state index I and refer to the current reference wavefunction as $|0\rangle$. Define the operator in the Bloch equation as

$$\hat{G} = \hat{H}_0 - E_0 + \epsilon_{\text{shift}} \tag{7}$$

The state-specific Bloch equation Eq.4 in the matrix form will be represented as

$$\mathbf{Gt} = \mathbf{h} \tag{8}$$

We will first focus on the 2nd order energy without level shift correction, which can be written in matrix form as

$$E^{\text{PT2}} = -\mathbf{t}^T \cdot \mathbf{h} = -\mathbf{h}^T \cdot \mathbf{G}^{-1} \cdot \mathbf{h} \tag{9}$$

In the original paper, we construct the basis functions $|\chi_n\rangle$ using internally contracted double excitations defined in spin orbitals. However, as mentioned in the introduction, the first order interacting space is spanned only by singlet-adapted double excitations on the reference wavefunction. Furthermore, one can further define the symmetric singlet-adapted double excitations:[57]

$$|\tilde{\chi}^{(+)}_{p_1h_1p_2h_2}\rangle = \frac{1}{2}\left(\hat{E}_{p_1h_1}\hat{E}_{p_2h_2} + \hat{E}_{p_1h_2}\hat{E}_{p_2h_1}\right)|0\rangle \tag{10}$$

and the antisymmetric singlet-adapted double excitations:

$$|\tilde{\chi}^{(-)}_{p_1h_1p_2h_2}\rangle = \frac{1}{2\sqrt{3}}\left(\hat{E}_{p_1h_1}\hat{E}_{p_2h_2} - \hat{E}_{p_1h_2}\hat{E}_{p_2h_1}\right)|0\rangle \tag{11}$$

Once $\left\{|\tilde{\chi}^{(+)}_{p_1h_1p_2h_2}\rangle, |\tilde{\chi}^{(-)}_{p_1h_1p_2h_2}\rangle\right\}$ are constructed, an orthonormalization step is then applied to create the final set of $\{|\chi_n\rangle\}$.

When the zeroth order $|0\rangle$ and $\hat{H}_0$ are from closed-shell Hartree-Fock calculations, the Bloch equation becomes diagonal and is trivial to solve, leading to the well-known closed

form MP2 energy expression. In contrast, the Bloch equation for CASPT2 is not diagonal, and we attribute this into two sources, i.e. "same-site" and "inter-site" interactions. To help explain the concepts, here we first use single excitations as a simpler example and consider a general one-electron operator $\hat{A}$. Let h denote the hole index that is created in the active or closed space, and let p denote the particle index that is created in the active or virtual space. Treat each index in the excitations as one "site". The couplings between single excitations under $\hat{A}$ can be decomposed in the following form:

$$\langle 0|\hat{E}^{\dagger}_{ph}\hat{A}\hat{E}_{p'h'}|0\rangle = [\bar{\alpha}_{pp'}\delta_{hh'} + \delta_{pp'}\alpha_{hh'}] + \Delta_{\text{inter}} \tag{12}$$

Based on the above decomposition, off-diagonal elements in the matrix of $\langle 0|\hat{E}^{\dagger}_{p'h'}\hat{O}\hat{E}_{ph}|0\rangle$ can arise from two sources. One source is the term in the square bracket of Eq.12 , where $\alpha_{h'h}$ couples a pair of hole indices and $\bar{\alpha}_{p'p}$ couples a pair of particle indices

$$\alpha_{hh'} = \frac{1}{2}\left[\langle 0|\hat{a}^{\dagger}_{h\alpha}\hat{A}\hat{a}_{h'\alpha}|0\rangle + \langle 0|\hat{a}^{\dagger}_{h\beta}\hat{A}\hat{a}_{h'\beta}|0\rangle\right] \tag{13}$$

$$\bar{\alpha}_{pp'} = \frac{1}{2}\left[\langle 0|\hat{a}_{p\alpha}\hat{A}\hat{a}^{\dagger}_{p'\alpha}|0\rangle + \langle 0|\hat{a}_{p\beta}\hat{A}\hat{a}^{\dagger}_{p'\beta}|0\rangle\right] \tag{14}$$

This term will be called "same-site interactions" since the off-diagonal coupling allows only one index to differ between the two excitations while the other indices must be identical. The second source is the Δ_{inter} term in Eq.12 , which will be called the "inter-site interactions" and is defined simply as the difference

$$\Delta_{\text{inter}} = \langle 0|\hat{E}^{\dagger}_{p'h'}\hat{O}\hat{E}_{ph}|0\rangle - [\bar{\alpha}_{p'p}\delta_{h'h} + \delta_{p'p}\alpha_{h'h}] \tag{15}$$

The existence of "inter-site interactions" is primarily due to that excitations in active space are all coupled together by the multi-reference effects.

By generalizing the above idea to double excitations, we can now decompose the Bloch equation as

$$\begin{gathered}\langle \chi^{(\sigma)}_{p_1h_1p_2h_2}|\hat{G}|\chi^{(\sigma)}_{p'_1h'_1p'_2h'_2}\rangle = [\bar{\gamma}_{p_1p'_1}\delta_{h_1h'_1}\delta_{p_2p'_2}\delta_{h_2h'_2} \\ \delta_{p_1p'_1}\gamma_{h_1h'_1}\delta_{p_2p'_2}\delta_{h_2h'_2} + \delta_{p_1p'_1}\delta_{h_1h'_1}\bar{\gamma}_{p_2p'_2}\delta_{h_2h'_2} + \delta_{p_1p'_1}\delta_{h_1h'_1}\delta_{p_2p'_2}\gamma_{h_2h'_2}] + \Delta_{\text{inter}}\end{gathered} \tag{16}$$

where the "single hole coupling matrix" is defined as

$$\gamma_{hh'} = \frac{1}{2}\left[\langle 0|\hat{a}^\dagger_{h\alpha}\hat{G}\hat{a}_{h'\alpha}|0\rangle + \langle 0|\hat{a}^\dagger_{h\beta}\hat{G}\hat{a}_{h'\beta}|0\rangle\right] \tag{17}$$

and the "single particle coupling matrix" is defined as

$$\bar{\gamma}_{pp'} = \frac{1}{2}\left[\langle 0|\hat{a}_{p\alpha}\hat{G}\hat{a}^\dagger_{p'\alpha}|0\rangle + \langle 0|\hat{a}_{p\beta}\hat{G}\hat{a}^\dagger_{p'\beta}|0\rangle\right] \tag{18}$$

The two terms in Eq.16 thus show how the off-diagonal elements in the Bloch equation are attributed to the same-site intersections (terms in the square bracket) and inter-site interactions (Δ_{inter}) respectively.

The main objective behind the supporting subspace factorization is to find a connection between CASPT2 energy with the MP2 energy expression. The above analysis suggests that to achieve this goal, it is necessary to remove or simplify both the same-site interactions as well as the inter-site interactions. These provide the motivations for the new derivations of spin-free supporting subspace factorization.

C. Remove the same site interactions through Kronecker sum when inter-site interactions are absent

Instead of considering both the same-site and inter-site interactions simultaneously, we will first consider an approximate system that neglects all inter-site interactions (i.e. in let $\Delta_{\text{inter}} \approx 0$ in Eq.16), and see how the same-site interactions can be removed in this simpler situation. Ideas and derivations in this subsection are similar to the original work, but everything is redefined in in the spin-free formulation.

Denote such approximate operator without inter-site interactions as $\hat{G}_{\text{apx}}$. The example of single excitations in Eq.15 gets simplified into

$$\langle 0|\hat{E}^\dagger_{ph}\hat{G}_{\text{apx}}\hat{E}_{p'h'}|0\rangle = \bar{\gamma}_{pp'}\delta_{hh'} + \delta_{pp'}\gamma_{hh'} \tag{19}$$

Using Kronecker sum[59] that was applied in the original paper

$$\mathbf{A} \oplus_K \mathbf{B} = \mathbf{A} \otimes \mathbf{I} + \mathbf{I} \otimes \mathbf{B} \tag{20}$$

Eq.19 can be expressed as

$$\langle 0|\hat{E}^{\dagger}_{ph}\hat{G}_{\mathrm{apx}}\hat{E}_{p'h'}|0\rangle = \bar{\gamma}_{pp'} \oplus_K \gamma_{hh'} \tag{21}$$

This idea can be generalized to spin-adapted double excitations (Eq.16) as

$$\langle \chi^{(\sigma)}_{p_1h_1p_2h_2}|\hat{G}_{\mathrm{apx}}|\chi^{(\sigma')}_{p'_1h'_1p'_2h'_2}\rangle = \delta_{\sigma\sigma'} \cdot \left(\bar{\gamma}_{p_1p'_1} \oplus_K \gamma_{h_1h'_1} \oplus_K \bar{\gamma}_{p_2p'_2} \oplus_K \gamma_{h_2h'_2}\right) \tag{22}$$

σ, σ' denote the symmetry $+$ or $-$ of the double excitations (see Eq.10 and Eq.11). The application of Kronecker sum in the absence of inter-site interactions is consistent with the physical interpretation of Kronecker sum: if two subsystems A and B are decoupled under an operator $\hat{O}$, then the representation of $\hat{O}$ in the full system can be written as Kronecker sum of representations of the two subsystems.[60]

The eigendecomposition property of Kronecker sum[59] can then be used to remove the same-site interactions. If the eigendecompositions of $\mathbf{A}$ and $\mathbf{B}$ in Eq.20 are known,i.e.

$$\mathbf{A} = \sum_i \mathbf{U}_i^T \lambda_i \mathbf{U}_i, \mathbf{B} = \sum_i \mathbf{V}_i^T \omega_i \mathbf{V}_i \tag{23}$$

then the eigenspectrum of kronecker sum $\mathbf{A} \oplus_K \mathbf{B}$ can be easily constructed as

$$\mathbf{A} \oplus_K \mathbf{B} = \sum_i \left(\mathbf{U}_i \otimes \mathbf{V}_i\right)^T \cdot (\lambda_i + \omega_i) \cdot (\mathbf{U}_i \otimes \mathbf{V}_i) \tag{24}$$

This suggests that we should first diagonalize the single hole and single particle coupling matrices (Eq.17 and 18) repectively,

$$\gamma_{hh'} = \sum_{\eta} T_{\eta h}(-\omega_\eta) T_{\eta h'} \tag{25}$$

$$\bar{\gamma}_{pp'} = \sum_{\pi} \bar{T}_{\pi p} \bar{\omega}_{\pi} \bar{T}_{\pi p'} \tag{26}$$

The operator $\hat{G}_{\text{apx}}$ then becomes diagonal in the transformed representation, i.e.

$$\langle \chi^{(\sigma)}_{\pi_1 \eta_1 \pi_2 \eta_2} | \hat{G}_{\text{apx}} | \chi^{(\sigma')}_{\pi'_1 \eta'_1 \pi'_2 \eta'_2} \rangle = \delta_{\sigma\sigma'} \cdot \delta_{\pi_1 \pi'_1} \delta_{\eta_1 \eta'_1} \delta_{\pi_2 \pi'_2} \delta_{\eta_2 \eta'_2} \cdot (\bar{\omega}_{\pi_1} - \omega_{\eta_1} + \bar{\omega}_{\pi_2} - \omega_{\eta_2}) \tag{27}$$

When the reference wavefunction is singlet, Eq.25 is equivalent to the dressed hole orbitals defined the original paper. However, due to the usage of spin orbitals in the original paper, when alpha and beta electrons are not equivalent (e.g. doublet states), the original approach will lead to two sets of dressed hole orbitals from diagonalizing the alpha-hole coupling matrix $\gamma^{\alpha}_{hh'} = \langle 0 | a^{\dagger}_{h\alpha} \hat{G} \hat{a}_{h'\alpha} | 0 \rangle$ and the beta-hole coupling matrix $\gamma^{\beta}_{hh'} = \langle 0 | a^{\dagger}_{h\beta} \hat{G} \hat{a}_{h'\beta} | 0 \rangle$ respectively. This is undesired as it notably increases the computational cost. With the usage of spin-adapted double excitation, the hole coupling matrix $\gamma_{hh'}$ in Eq.17 is defined in a spin-averaged form, thus can be applied to any spin states. Similarly, Eq.26 is equivalent to the dressed particle orbitals defined in the original paper for singlet states, but further generalize the concept to any spin states.

The fact that same-site interactions can be effectively removed for $\hat{G}_{\text{apx}}$ by transforming into the dressed representation (Eq.27) suggests that the corresponding second order energy can be easily computed in the dressed representation. Denote the Bloch equation using $\hat{G}_{\text{apx}}$ as

$$\mathbf{G}_{\text{apx}} \mathbf{t}_{\text{apx}} = \mathbf{h}_{\text{apx}} \tag{28}$$

Approximate the right hand side of the Bloch equation $\mathbf{h}_{\text{apx}}$ as

$$\langle 0 | \hat{H}_{\text{approx}} | \chi^{(+)}_{h_1 p_1 h_2 p_2} \rangle = (h_1 p_1 | h_2 p_2) + (h_1 p_2 | h_2 p_1) \tag{29}$$

$$\langle 0 | \hat{H}_{\text{approx}} | \chi^{(-)}_{h_1 p_1 h_2 p_2} \rangle = \sqrt{3} \left[(h_1 p_1 | h_2 p_2) - (h_1 p_2 | h_2 p_1) \right] \tag{30}$$

where $(pq|rs) = \int \phi_p(r) \phi_q(r) \frac{1}{|\mathbf{r}_1 - \mathbf{r}_2|} \phi_r(\mathbf{r}_2) \phi_s(\mathbf{r}_2) d\mathbf{r}_1 d\mathbf{r}_2$ is the two-electron repulsion integrals. The approximate second order energy can then be computed as

$$E^{\text{PT2}}_{\text{apx}} = -\mathbf{h}^T_{\text{apx}} \cdot \mathbf{G}^{-1}_{\text{apx}} \cdot \mathbf{h}_{\text{apx}} \tag{31}$$

By transforming into the dressed representation, Eq.27 suggests that $\hat{G}^{-1}_{\text{apx}}$ becomes diagonal

$$\langle \chi^{(\sigma)}_{\pi_1\eta_1\pi_2\eta_2} | \hat{G}^{-1}_{\text{apx}} | \chi^{(\sigma')}_{\pi'_1\eta'_1\pi'_2\eta'_2} \rangle = \delta_{\sigma\sigma'} \cdot \delta_{\pi_1\pi'_1}\delta_{\eta_1\eta'_1}\delta_{\pi_2\pi'_2}\delta_{\eta_2\eta'_2} \cdot (\bar{\omega}_{\pi_1} - \omega_{\eta_1} + \bar{\omega}_{\pi_2} - \omega_{\eta_2})^{-1} \tag{32}$$

thus $E^{\text{CASPT2}}_{\text{apx}}$ takes the simple form of MP2 energy expression

$$E^{\text{CASPT2}}_{\text{apx}} = E^{\text{MP2}}_{\text{dressed}} = -\sum_{\pi_1\eta_1\pi_2\eta_2} \frac{(\pi_1\eta_1|\pi_2\eta_2)\left[2(\pi_1\eta_1|\pi_2\eta_2) - (\pi_1\eta_2|\pi_2\eta_1)\right]}{\bar{\omega}_{\pi_1} - \omega_{\eta_1} + \bar{\omega}_{\pi_2} - \omega_{\eta_2}} \tag{33}$$

Eq.33 is equivalent to the the dressed MP2 energy introduced in the original paper for singlet states, but now can be applied to arbitrary spin states because the dressed orbitals are defined in a spin-averaged manner. As one of the simplest correlation methods, there have been extensive research on high performance implementations for MP2 calculations, and the above expression allows CASPT2 to benefit from these MP2 codes.

Although $\hat{G}^{-1}_{\text{apx}}$ defined in the dressed representation (Eq.32) is the most convenient, we often need $\hat{G}^{-1}_{\text{apx}}$ in the original representation in later discussions. To obtain a factorized form, first apply Laplace transformation to the energy denominators in Eq.32

$$\frac{1}{\bar{\omega}_{\pi_1} - \omega_{\eta_1} + \bar{\omega}_{\pi_2} - \omega_{\eta_2}} = \sum_{\kappa} \bar{\tau}^{(\kappa)}_{\pi_1} \tau^{(\kappa)}_{\eta_1} \bar{\tau}^{(\kappa)}_{\pi_2} \tau^{(\kappa)}_{\eta_2} \tag{34}$$

where $\tau^{(\kappa)}_{\eta} = e^{\omega_\eta t_{(\kappa)}}$ and $\bar{\tau}^{(\kappa)}_{\pi} = e^{-\bar{\omega}_\pi t_{(\kappa)}}$ for the κ-th quadrature point $t_{(\kappa)}$. The property of Kronecker sum in Eq.24 allows $\mathbf{G}^{-1}_{\text{apx}}$ in the original representation to be factorized as

$$\mathbf{G}^{-1}_{\text{apx}} = \sum_{\kappa} \bar{\mathbf{M}}^{(\kappa)} \otimes \mathbf{M}^{(\kappa)} \otimes \bar{\mathbf{M}}^{(\kappa)} \otimes \mathbf{M}^{(\kappa)} \tag{35}$$

where the matrices $\mathbf{M}^{(\kappa)}$ and $\bar{\mathbf{M}}^{(\kappa)}$ are computed using the transformation matrices (see Eq.25 and Eq.26) as

$$M^{(\kappa)}_{hh'} = \sum_{\eta} T_{\eta h} \tau^{(\kappa)}_{\eta} T_{\eta h'} \tag{36}$$

$$\bar{M}^{(\kappa)}_{pp'} = \sum_{\pi} \bar{T}_{\pi p} \bar{\tau}^{(\kappa)}_{\pi} \bar{T}_{\pi p'} \tag{37}$$

The factorized form of $\mathbf{G}^{-1}_{\text{apx}}$ in Eq.35 will play an important role in the next section. The Laplace transformation in Eq.34 requires that the energy denominators in the dressed or-

bitals ($\bar{\omega}_{\pi_1} - \omega_{\eta_1} + \bar{\omega}_{\pi_2} - \omega_{\eta_2}$) all have postive values. However, we do observe that they can contain a few negative values even when the exact Bloch equation is postive definite and well-conditioned, which indicates that they result from the neglects of inter-state interactions instead of the presence of intruder-states, and will be removed once the inter-state interactions are recovered. A remedy approach for treating these negative energy denominators has been developed in our previous work,[52] which requires computational cost approximately equivalent to adding one additional quadrature point.

The success of Kronecker sum used in this Section relies on the fact that the diagonal elements of the approximate Bloch equation $\mathbf{G}_{\text{apx}}$ can be decomposed in the summation form of $\bar{\lambda}_{p_1} + \lambda_{h_1} + \bar{\lambda}_{p_2} + \lambda_{h_2}$. The real level shift[17] used in this work is compatible with this requirement, since it simply shifts each $\bar{\lambda}_p$ and λ_h by a constant $\epsilon_{\text{shift}}/4$. However, real level shift does not truly remove the singularity and is known to have problem for systems like transition metal complex with a dense group of electronic excited states all close in energy. In these situations, one should use approaches such as imaginary shift[61,62] or σ^p-regularization[19] for reliable intruder-state removal. Unfortunately, the approach used in this work is currently not compatible with these improved level shift techniques. As an example, the imaginary shift effectively modifies a diagonal element $\Delta_{p_1h_1p_2h_2}$ into $\Delta_{p_1h_1p_2h_2} + \frac{\epsilon^2_{\text{shift}}}{\Delta_{p_1h_1p_2h_2}}$, and we haven't found a way to decompose this expression into the desired summation form. Given the drawback, it is worth developing intruder-state removal method that is compatible with the Kronecker sum in the future in order to make supporting subspace factorization applicable to a wider range of systems.

It is also worth mentioning that the approach used in this section is conceptually different from the diagonal approximation of CASPT2 (D-CASPT2)[14]. In D-CASPT2, the Bloch equation is approximated to be diagonal in the original representation. In contrast, the approximated Bloch equation in this section still contains off-diagonal elements in the original representation that arise from the same-site interaction as shown by Eq.22. The Bloch equation only becomes diagonal in the dressed representation through the transformation matrices $T_{\eta h}$ and $\bar{T}_{\pi p}$ defined in Eq.25 and Eq.26 respectively.

D. Recover the inter-site interactions through Löwdin Partition

The above idea of capturing multi-reference effects through single reference method in dressed orbitals is certainly not new.[63,64] However, our original paper showed that keeping only the $E^{\mathrm{MP2}}_{\mathrm{dressed}}$ term as defined in Eq.33 while neglecting all the inter-site interactions can give qualitatively wrong potential energy curves when the molecule is in region with strong static correlation. This suggests that it is critical to account for the inter-site interactions in order to obtain accurate descriptions of the potential energy surfaces.

In this section, we will show how the inter-site interactions can be *exactly* recovered through Löwdin partition.[65] One benefit from using Löwdin partition is that the dimension of the effective linear system in the subspace becomes significantly smaller than the original linear equation. As a result, to exactly recover the inter-site interactions only requires operations that scale as $O(N^3)$ with respect to number of atomic orbitals for a given active space settings. The derivations in this section are fundamentally different from the original work, and will reveal the physical meanings of supporting subspace factorization along the way.

1. Partition of first order interacting space

In previous studies of CASPT2, the first order interacting space is often partitioned primarily based on the number of excited electrons in the external orbitals (i.e. virtual orbitals), and is thus partitioned into the internals $|I\rangle$, semi-internals (also called singles) $|S^a\rangle$, and externals (also called doubles) $|D^{ab}\rangle$ with 0, 1 and 2 external electrons respectively.[16,66,67] Furthermore, based on the number of holes in the closed orbitals, each subspace can be further partitioned as $|I\rangle \in \{I_0, I_1, I_2\}$, $|S^a\rangle \in \{S^a_0, S^a_1, S^a_2\}$ and $|D^{ab}\rangle \in \left\{D^{ab}_0, D^{ab}_1, D^{ab}_2\right\}$, where subscripts denote the numbers of holes in the closed orbitals. Note that because complete active space spans I_0, it does not contribute to CASPT2 calculations, but should be included if the reference is from restricted active space (RAS) calculation.

Even though inter-site interactions cannot be neglected for the entire first-order interacting space, it is strictly zero within certain subspace. As explained in SI-Section 1.1, inter-site interactions do not exist (i.e. $\Delta_{\mathrm{inter}} = 0$ in Eq.16) for $\langle \chi^{(\sigma)}_{p_1 h_1 p_2 h_2} | \hat{G} | \chi^{(\sigma')}_{p'_1 h'_1 p'_2 h'_2} \rangle$ if for both the bra and the ket, each double excitation involves three or four indices outside the active space.

As a result, instead of partitioning the space based primarily on the external electrons, we will partition the first-order interacting space based on both the number of electrons in the virtual orbitals and the number of holes in the closed orbitals. Based on this property, we define the leading subspace to comprise of all double excitations with three or four indices in the virtual or closed orbitals, and the projection operator to the leading subspace P_L is defined as

$$P_L = \sum_{abij} |D_{ij}^{ab}\rangle\langle D_{ij}^{ab}| + \sum_{abi} |D_{i}^{ab}\rangle\langle D_{i}^{ab}| + \sum_{aij} |S_{ij}^{a}\rangle\langle S_{ij}^{a}| \tag{38}$$

where the three terms represent projection into the subspaces D_2^{ab}, D_1^{ab} and S_2^a respectively. By definition, $\mathbf{G_{apx}}$ and $\mathbf{G}$ are connected as

$$P_L \mathbf{G}_{\text{apx}} P_L = P_L \mathbf{G} P_L \tag{39}$$

In addition, SI-Section 1.1 shows that $\mathbf{h}_{\text{apx}}$ in Eq.29 and Eq.30 are chosen such that

$$P_L \mathbf{h}_{\text{apx}} = P_L \mathbf{h} \tag{40}$$

The symmetric and antisymmetric excitations in the leading subspace are decoupled under $\hat{G}$, thus we can further decompose the projection operator as $P_L = P_L^{(+)} + P_L^{(-)}$.

Given the definition of the leading subpace, the supporting subspace is defined as the remaining first order interaction space of $\hat{G}_{\text{apx}}$, i.e.

$$Q_S \mathbf{G}_{\text{apx}} Q_S = (1 - P_L)\mathbf{G}_{\text{apx}}(1 - P_L) \tag{41}$$

The symmetric and antisymmetric double excitations in the supporting subspace are also decoupled under $\hat{G}_{\text{apx}}$, and we can further write $Q_S = Q_S^{(+)} + Q_S^{(-)}$. Similarly, the trailing subspace is defined as the remaining first order interaction space of the true operator $\hat{G}$.

$$Q_T \mathbf{G} Q_T = (1 - P_L)\mathbf{G}(1 - P_L) \tag{42}$$

However, the symmetric and antisymmetric double excitations in the trailing subspace are no longer decoupled under $\hat{G}$.

Figure 1 illustrates the partition of $\mathbf{G}$ into the leading and trailing subspace $P_L + Q_T$, and the partition of $\mathbf{G}_{\text{apx}}$ into the leading and supporting subspace $P_L + Q_S$. With the partition of space, the Löwdin partition becomes the natural tool to find the corresponding partition of energy. Mathematically, this is equivalent to the Block Gaussian elimination used in the original paper. In general, suppose a linear equation $\mathbf{Ax} = \mathbf{b}$ can be partitioned as

$$\begin{pmatrix} P\mathbf{A}P & P\mathbf{A}Q \\ Q\mathbf{A}P & Q\mathbf{A}Q \end{pmatrix} \begin{pmatrix} P\mathbf{x} \\ Q\mathbf{x} \end{pmatrix} = \begin{pmatrix} P\mathbf{b} \\ Q\mathbf{b} \end{pmatrix} \tag{43}$$

where P and Q are projection operators $P + Q = I$ that need to be defined specifically for each problem. Below we summarize the main conclusions from Löwdin partition, and the detailed derivations can be found in SI-Section 1.2. The total energy can be partitioned as

$$E_{\text{total}} = E_P + E_Q^{\text{eff}} \tag{44}$$

E_P involves interactions only within the P space, and is defined as

$$E_P = -\left(P\mathbf{b}\right)^T \cdot \left(P\mathbf{A}P\right)^{-1} \cdot \left(P\mathbf{b}\right) \tag{45}$$

E_Q^{eff} contains all the remaining energy

$$E_Q^{\text{eff}} = -\left(Q\mathbf{b}^{\text{eff}}\right)^T \cdot \left(Q\mathbf{x}\right) \tag{46}$$

The effective vector $\mathbf{b}^{\text{eff}}$ has embedded effects from the P space and is expressed as

$$\mathbf{b}^{\text{eff}} = \mathbf{b} - \mathbf{A}P\left(P\mathbf{A}P\right)^{-1} P\mathbf{b} \tag{47}$$

and satisfies $P\mathbf{b}^{\text{eff}} = 0$. The vector $Q\mathbf{x}$ can be solved from the following linear equation

$$\left(Q\mathbf{A}^{\text{eff}}Q\right) \cdot \left(Q\mathbf{x}\right) = Q\mathbf{b}^{\text{eff}} \tag{48}$$

where $\mathbf{A}^{\text{eff}}$ has also embedded effects from the P space as

$$\mathbf{A}^{\text{eff}} = \mathbf{A} - \mathbf{A}P\left(P\mathbf{A}P\right)^{-1}P\mathbf{A} \tag{49}$$

and satisfies

$$Q\mathbf{A}^{\text{eff}}Q = \left(Q\mathbf{A}^{-1}Q\right)^{-1} \tag{50}$$

$\mathbf{A}^{\text{eff}}$ also statisfies $P\mathbf{A}^{\text{eff}}P = P\mathbf{A}^{\text{eff}}Q = Q\mathbf{A}^{\text{eff}}P = 0$. Note that the dimension of the effective linear system Eq.48 in the subspace Q is smaller than the original linear system. If $P\mathbf{x}$ is needed explicitly, it can be computed from $Q\mathbf{x}$ as

$$P\mathbf{x} = \left(P\mathbf{A}P\right)^{-1}P\left(\mathbf{b} - \mathbf{A}Q\mathbf{x}\right) \tag{51}$$

In addition to the above general conclusions, we have also found the following properties if $\mathbf{A}^{-1}$ is easy to compute (e.g. $\mathbf{G}_{\text{apx}}^{-1}$ in Eq.35). If $\mathbf{A}^{-1}$ is already known, $(Q\mathbf{x})$ can be directly expressed as

$$Q\mathbf{x} = Q\mathbf{A}^{-1}\mathbf{b} \tag{52}$$

By substituting Eq.52 and Eq.50 into Eq.48, instead of using Eq.47, $Q\mathbf{b}^{\text{eff}}$ can be solved from the following linear equation instead

$$\left(Q\mathbf{A}^{-1}Q\right)\cdot\left(-Q\mathbf{b}^{\text{eff}}\right) = -\left(Q\mathbf{A}^{-1}\mathbf{b}\right) \tag{53}$$

A negative sign is added to be consistent with later derivations (see Eq.62). In addition, we will often encounter $(P\mathbf{A}P)^{-1}P\mathbf{b}$, or matrix-vector product in the general form of $(P\mathbf{A}P)^{-1}P\mathbf{v}$ for an arbitrary vector $\mathbf{v}$ (such as Eq.51). From Eq.47,

$$\left(P\mathbf{A}P\right)^{-1}P\mathbf{b} = \mathbf{A}^{-1}\left[\mathbf{b} + \left(-Q\mathbf{b}^{\text{eff}}\right)\right] \tag{54}$$

The same idea in Eq.54 and Eq.53 can be applied to $(P\mathbf{A}P)^{-1}P\mathbf{v}$ by replacing $\mathbf{b}$ with $\mathbf{v}$, and this will become powerful tools for computing such matrix vector product if $\mathbf{A}^{-1}$ is trivial.

By applying Eq.44 to the partition of the approximate Bloch equation (Eq.28) into leading

and supporting subspace, we have

$$E_{\text{apx}}^{\text{CASPT2}} = E_{\text{dressed}}^{\text{MP2}} = \tilde{E}_L + E_S^{\text{eff}} \tag{55}$$

and from Eq.45

$$\tilde{E}_L = -\left(P\mathbf{h}_{\text{apx}}\right)^T \cdot \left(P\mathbf{G}_{\text{apx}}P\right)^{-1} \cdot \left(P\mathbf{h}_{\text{apx}}\right) \tag{56}$$

Similarly, by applying Eq.44 to the partition of the true Bloch equation (Eq.8) into leading and trailing subspace, we have

$$E^{\text{CASPT2}} = E_L + E_T^{\text{eff}} \tag{57}$$

and from Eq.45

$$E_L = -\left(P\mathbf{h}\right)^T \cdot \left(P\mathbf{G}P\right)^{-1} \cdot \left(P\mathbf{h}\right) \tag{58}$$

By the definition of leading space in Eq.39 and Eq.40,

$$\tilde{E}_L = E_L \tag{59}$$

The true CASPT2 energy in Eq.57 is thus related to the dressed MP2 energy in Eq.55 as

$$E^{\text{CASPT2}} = E_{\text{dressed}}^{\text{MP2}} - E_S^{\text{eff}} + E_T^{\text{eff}} \tag{60}$$

Therefore, in order to compute the true CASPT2 energy from the dressed MP2 energy, we need to first remove fictitious contributions from the supporting subspace $-E_S^{\text{eff}}$ then add back the true contributions from the trailing subspace $+E_T^{\text{eff}}$. Evaluations of E_S^{eff} and E_T^{eff} will be discussed in the next two sections respectively.

It is worth pointing out that the above definitions of the leading subspace, supporting subspace, and trailing subspace are all consistent with what were proposed in the original paper for singlet states, although the original paper was primarily based on considerations of computational cost. As indicated in Figure 1, given an active space setting, the size of tensors in the leading subspace increases as high as $O(N^4)$ with the number of atomic orbitals, while those in the supporting subspace or trailing subspace increase at most as $O(N^2)$ with the number of atomic orbitals. As a result, the dimension of the effective linear equation (Eq.48)

defined in the supporting or trailing subspace is much smaller compared to the true Bloch equation, which lays the foundation for reduction in both memory requirement and floating point operations.

2. *Supporting subspace contribution* E_S^{eff}

To compute the supporting subspace contribution E_S^{eff}, apply Eq.46 from Löwdin partition to the approximate Bloch equation Eq.28, i.e. let $\mathbf{A} = \mathbf{G}_{\text{apx}}$ and $\mathbf{b} = \mathbf{h}_{\text{apx}}$

$$E_S^{\text{eff}} = -\left(Q_S \mathbf{h}_{\text{apx}}^{\text{eff}}\right)^T \cdot (Q_S \mathbf{t}_{\text{apx}}) \tag{61}$$

Because the symmetric and antisymmetric excitations are decoupled under $\hat{G}_{\text{apx}}$, by defining

$$\mathbf{s}_{\text{apx}}^{(\sigma)} = -Q_S^{(\sigma)} \mathbf{h}_{\text{apx}}^{\text{eff}} \tag{62}$$

we can further separate the above energy based on symmetry as

$$E_S^{\text{eff}} = \sum_{\sigma=+,-} E_S^{\text{eff}(\sigma)} = \sum_{\sigma=+,-} \left(\mathbf{s}_{\text{apx}}^{(\sigma)}\right)^T \cdot \left(Q_S^{(\sigma)} \mathbf{t}_{\text{apx}}\right) \tag{63}$$

To evaluate the quantities needed in Eq.63, we will take advantage of the fact that $\mathbf{G}_{\text{apx}}^{-1}$ is easy to evaluate as factorized in Eq.35. This allows $Q_S^{(\sigma)} \mathbf{t}_{\text{apx}}$ to be computed following Eq.52

$$Q_S^{(\sigma)} \mathbf{t}_{\text{apx}} = Q_S^{(\sigma)} \mathbf{G}_{\text{apx}}^{-1} \mathbf{h}_{\text{apx}} \tag{64}$$

With $\mathbf{G}_{\text{apx}}^{-1}$ known, it also allows $\mathbf{s}_{\text{apx}}^{(\sigma)} = -\left(Q_S^{(\sigma)} \mathbf{h}_{\text{apx}}^{\text{eff}}\right)$ to be solved based on Eq.53, which leads to the following linear equation that can be solved iteratively using preconditioned conjugate gradient

$$\left(Q_S^{(\sigma)} \mathbf{G}_{\text{apx}}^{-1} Q_S^{(\sigma)}\right) \cdot \mathbf{s}_{\text{apx}}^{(\sigma)} = -Q_S^{(\sigma)} \mathbf{G}_{\text{apx}}^{-1} \mathbf{h}_{\text{apx}} \tag{65}$$

It turns out that the linear equation Eq.65 takes the same form as the "supporting tensor solver" in the original paper for singlet states if $Q_S^{(\sigma)}$ is replaced with Q_S. This suggests that $\mathbf{s}_{\text{apx}}^{(\sigma)}$ defined in Eq.62 plays the same role as the supporting tensor introduced in the original paper. In contrast to the original paper that merely introduced the supporting tensor as

a mathematical trick, the definition in Eq.62 clearly shows how the supporting tensor can naturally arise from the Löwdin partition.

3. *Trailing subspace contribution* E_T^{eff}

To compute the trailing subspace contribution E_T^{eff}, apply Eq.46 from Löwdin partition to the true Bloch equation Eq.8, i.e. let $\mathbf{A} = \mathbf{G}$ and $\mathbf{b} = \mathbf{h}$

$$E_T^{\text{eff}} = -\left(Q_T \mathbf{h}^{\text{eff}}\right)^T \cdot \left(Q_T \mathbf{t}\right) \tag{66}$$

Based on Eq.47 from the Löwdin partition and $P_L = P_L^{(+)} + P_L^{(-)}$, we have

$$Q_T \mathbf{h}^{\text{eff}} = Q_T \mathbf{h} - \sum_{\sigma=+,-} \left(Q_T \mathbf{G} P_L^{(\sigma)}\right) \left(P_L^{(\sigma)} \mathbf{G} P_L^{(\sigma)}\right)^{-1} \mathbf{h} \tag{67}$$

Based on Eq.48, $Q_T \mathbf{t}$ can be solved from

$$\left(Q_T \mathbf{G}^{\text{eff}} Q_T\right) \left(Q_T \mathbf{t}\right) = \left(Q_T \mathbf{h}^{\text{eff}}\right) \tag{68}$$

In order to solve Eq.68 using preconditioned conjugate gradient (PCG), each iteration requires building the matrix-vector product between $\left(Q_T \mathbf{G}^{\text{eff}} Q_T\right)$ and a trial vector. Denote the trivial vector at current iteration as $\mathbf{v}_{\text{trial}}$. From Eq.50 of Löwdin partition,

$$\begin{aligned} \left(Q_T \mathbf{G}^{\text{eff}} Q_T\right) \mathbf{v}_{\text{trial}} &= \left(Q_T \mathbf{G} Q_T\right) \mathbf{v}_{\text{trial}} \\ - \textstyle\sum_{\sigma=+,-} \left(Q_T \mathbf{G} P_L^{(\sigma)}\right) \left(P_L^{(\sigma)} \mathbf{G} P_L^{(\sigma)}\right)^{-1} &\left(P_L^{(\sigma)} \mathbf{G} Q_T \mathbf{v}_{\text{trial}}\right) \end{aligned} \tag{69}$$

The main difficulty of evaluating both Eq.67 and Eq.69 comes from $\left(P_L \mathbf{G} P_L\right)^{-1}$. Our general strategy will be to first use Eq.39 such that $\left(P_L \mathbf{G} P_L\right)^{-1}$ is replaced with $\left(P_L \mathbf{G}_{\text{apx}} P_L\right)^{-1}$. Since $\mathbf{G}_{\text{apx}}^{-1}$ is already known, it allows us to use the trick from Eq.54 and Eq.53 to compute its product with arbitrary vector.

To be more specific, use the fact that within the leading subspace, $\mathbf{G}$ is identical to $\mathbf{G}_{\text{apx}}$

(Eq.39), and $\mathbf{h}$ is identical to $\mathbf{h}_{\text{apx}}$(39)

$$\left(P_L^{(\sigma)}\mathbf{G}P_L^{(\sigma)}\right)^{-1}\mathbf{h}^{(\sigma)} = \left(P_L^{(\sigma)}\mathbf{G}_{\text{apx}}P_L^{(\sigma)}\right)^{-1}\mathbf{h}_{\text{apx}}^{(\sigma)} \tag{70}$$

The right hand side can now be evaluated using Eq.54 for $\mathbf{A}$ =$\mathbf{G}_{\text{apx}}$ and $\mathbf{b} = \mathbf{h}_{\text{apx}}$ as

$$\left(P_L^{(\sigma)}\mathbf{G}_{\text{apx}}P_L^{(\sigma)}\right)^{-1}\mathbf{h}_{\text{apx}}^{(\sigma)} = \mathbf{G}_{\text{apx}}^{-1}\left(\mathbf{h}_{\text{apx}}^{(\sigma)} + \mathbf{s}_{\text{apx}}^{(\sigma)}\right) \tag{71}$$

where we have used the definition of the supporting tensor (Eq.62). $Q_T\mathbf{h}^{\text{eff}}$ in Eq.67 can thus be computed as

$$Q_T\mathbf{h}^{\text{eff}} = Q_T\mathbf{h} - \sum_{\sigma=+,-}\left(Q_T\mathbf{G}P_L^{(\sigma)}\right)\cdot\mathbf{G}_{\text{apx}}^{-1}\left(\mathbf{h}_{\text{apx}}^{(\sigma)} + \mathbf{s}_{\text{apx}}^{(\sigma)}\right) \tag{72}$$

Similarly, in order to evaluate Eq.69, first solve the corresponding supporting tensor from

$$\left(Q_S^{(\sigma)}\mathbf{G}_{\text{apx}}^{-1}Q_S^{(\sigma)}\right)\cdot\mathbf{s}_{\text{trial}}^{(\sigma)} = -Q_S^{(\sigma)}\mathbf{G}_{\text{apx}}^{-1}\cdot\left(P_L^{(\sigma)}\mathbf{G}Q_T\right)\mathbf{v}_{\text{trial}} \tag{73}$$

The corresponding matrix vector product can then be computed as

$$\begin{array}{c}\left(Q_T\mathbf{G}^{\text{eff}}Q_T\right)\mathbf{v}_{\text{trial}} = \left(Q_T\mathbf{G}Q_T\right)\mathbf{v}_{\text{trial}} \\ -\sum_{\sigma=+,-}\left(Q_T\mathbf{G}P_L^{(\sigma)}\right)\mathbf{G}_{\text{apx}}^{-1}\left[P_L^{(\sigma)}\mathbf{G}Q_T\mathbf{v}_{\text{trial}} + \mathbf{s}_{\text{trial}}^{(\sigma)}\right]\end{array} \tag{74}$$

The above discussions show how the double excitation amplitudes in the trailing subspace $Q_T\mathbf{x}$ can be solved. In the situation that the entire wavefunction amplitudes are needed, based on Eq.51 in the Löwdin partition, $P_L\mathbf{x}$ is related to $Q_T\mathbf{x}$ as

$$P_L^{(\sigma)}\mathbf{t} = \left(P_L^{(\sigma)}\mathbf{G}P_L^{(\sigma)}\right)^{-1}\left(\mathbf{h}^{(\sigma)} - P_L^{(\sigma)}\mathbf{G}Q_T\mathbf{t}\right) \tag{75}$$

which again involves $\left(P_L\mathbf{G}P_L\right)^{-1}$. Using the same trick as Eq.72 and Eq.74, $P_L\mathbf{t}$ can be written as

$$P_L^{(\sigma)}\mathbf{t} = \mathbf{G}_{\text{apx}}^{-1}\left(\mathbf{h}_{\text{apx}}^{(\sigma)} + \mathbf{s}_{\text{apx}}^{(\sigma)} - P_L^{(\sigma)}\mathbf{G}Q_T\mathbf{t} - \mathbf{s}_t^{(\sigma)}\right) \tag{76}$$

where $\mathbf{s}_t^{(\sigma)}$ is solved from Eq.73 by letting $\mathbf{v}_{\text{trial}} = Q_T\mathbf{t}$. Eq.76 provides the full wavefunction

amplitude in the supporting subspace factorized form, which can then be used to compute the level-shift correction (last term in Eq.5) and off-diagonal element (Eq.5).

E. Implementation

The algorithm described above is summarized in Table I. The dressed MP2 energy can be evaluated using any standard single-reference MP2 codes. In this work, we use MP2 factorized with tensor hyper-contraction (THC). The main benefit of THC-MP2 is that it reduces the computational scaling of operations to $O(N^4)$ and the scaling of memory storage to $O(N^2)$ with increasing number of atomic orbitals.

In Table I, evaluation of the remaining terms other than the dressed MP2 energy involves three types of quantities. One is $\mathbf{h}^{(\sigma)}_{\mathrm{apx}}$ in Eq.29 and Eq.30 that take the form of ERIs. Second type consists of the supporting tensors $\mathbf{s}^{(\sigma)}_{\mathrm{apx}}$ and $\mathbf{s}^{(\sigma)}_{\mathrm{trial}}$. Third type consists of the trailing subspace tensors such as $Q_T\mathbf{t}$ and $Q_t\mathbf{h}^{\mathrm{eff}}$. Implementation of the algorithm involves transformations among these three types of quantities. Although tensors defined in the spin-free formulation have different values, they are of similar structure as the original spin-orbital formulation. This allows us to reuse the transformation operations already developed in the original paper, as described in the corresponding SI Sections listed in Table I. In particular, operations involving $\mathbf{h}_{\mathrm{apx}}$ can be formulated using Fock builds, while all other operations are formulated as basic linear algebra (BLAS) operations. As explained in SI-Section 1.3, each Fock build or BLAS operation formally scales as $O(N^3)$ with the number of atomic orbitals, and the number of such operations needed increases as n_{act}^2 with the number of active orbitals. The factor n_{act}^2 is related to the fact that double excitations in the supporting or trailing subspace involve at most two out of four indices outside the active space.

In addition, tensors defined in the spin-free formulation in this work possess symmetry, which is an additional advantage over the original paper. As already well-established in existing CASPT2 implementations, spin-coupled excitations can be defined for all doubly external excitations $|D^{ab}\rangle$ as well as internal excitations of type $|I_2\rangle$, leading to coefficient tensors that are either symmetric or antisymmetric with respect to permutation of indices.

This suggests that the supporting tensors have the symmetry that

$$s^{(\sigma)}_{p_1h_1p_2h_2} = (-1)^\sigma s^{(\sigma)}_{p_1h_2p_2h_1} = (-1)^\sigma s^{(\sigma)}_{p_2h_1p_1h_2} = s^{(\sigma)}_{p_2h_2p_1h_1} \tag{77}$$

Similarly, for the trailing subspace tensors, if two indices are both in the closed space or both in the virtual space, then

$$t^{(\sigma)}_{ij,D} = (-1)^\sigma t^{(\sigma)}_{ji,D}, t^{(\sigma)}_{ab,D} = (-1)^\sigma t^{(\sigma)}_{ba,D} \tag{78}$$

As shown in the example in SI-Section 1.3.3, the symmetry properties can help reduce the prefactor of computational cost by avoiding calculating all the elements explicitly.

III. RESULTS AND DISCUSSION

The method described in this work is implemented in the TERACHEM[68,69] quantum chemistry package. No frozen core approximation is used, i.e., all molecular orbitals are included in the perturbation calculations. A level shift parameter of 0.35 Hartree is used unless otherwise stated. The number of states included in the SA-CASSCF calculations is equal to the number of states computed in XMS-CASPT2. Geometry optimizations are carried out using the geomeTRIC software.[70] All calculations are performed on computing nodes with NVIDIA GeForce GTX 1080 Ti GPUs and Intel Xeon E5-2643 CPUs. Figures in the supplementary material will be referred to as SI-Figure.

A. Accuracy

To test the accuracy of the new method, the electronic excited state energies of a few test molecules are computed using both the supporting subspace XMS-CASPT2 (this work) as well as conventional XMS-CASPT2 (using BAGEL as the reference code). Figure 2 presents the potential energy curves for benzene along the reaction pathway that connects the Frank–Condon point (FC) and the S0/S1 minimum energy conical intersection (MECI). The energies from this work and energies from BAGEL are shifted by the same constant (S0 energy at the first image computed by BAGEL), thus the curves show direct comparison

bewteen the absolute energies. Both geometries at the end points are optimized using SA-CASSCF, and the geometries in between are generated through interpolation in the internal coordinates. The potential energy curves include 2 singlet states and 3 triplet states (using active space (6e, 6o)), as well as 3 doublet states and 3 quartet states (assuming benzene has been ionized, using active space (5e, 6o)). The maximum difference in the absolute energies between this work and the reference code is 0.0177 eV (0.408 kcal/mol). The good agreement can also be viewed directly from Figure 2 (a), which shows that all white dots (representing energies from conventional XMS-CASPT2) are right at the center of the solid colored dots (representing energies from supporting-subspace XMS-CASPT2).

To help understand the contribution from same-site and inter-site interactions respectively, based on Eq.60, we study how the potential energy curves change when the correlation energies are computed as $E^{\mathrm{MP2}}_{\mathrm{dressed}}$, $\left(E^{\mathrm{MP2}}_{\mathrm{dressed}} - E^{\mathrm{eff}}_{S}\right)$ and $\left(E^{\mathrm{MP2}}_{\mathrm{dressed}} - E^{\mathrm{eff}}_{S} + E^{\mathrm{eff}}_{T}\right)$ respectively. Figure 2 (b) shows how the state-specific CASPT2 potential energies (i.e. diagonal elements in the $\mathbf{H}^{\mathrm{eff}}$ in Eq.5 without level shift correction) change correspondingly for the singlet states as the geometries move from the Franck-Condon region to the conical intersection region. First, when inter-site interactions are neglected and the correlation energies are computed as $E^{\mathrm{MP2}}_{\mathrm{dressed}}$ (black), the results are qualitatively wrong and fail to describe the conical intersections. This is consistent with the understanding that inter-site interactions are most prominent where static correlation is strong, as also observed for twisted ethylene in our previous work.[51] In addition, a small jump appears around image 56 due to negative energy denominators in the dressed orbitals, which will be removed once inter-site interactions are recovered. In future works, it is worth studying whether it is possible to prevent these negative denominators through improved level-shift techniques. Second, after removing the contribution from the supporting subspace through $\left(E^{\mathrm{MP2}}_{\mathrm{dressed}} - E^{\mathrm{eff}}_{S}\right)$ (magneta), the shapes of the potential energy curves become qualitatively correct. This is equivalent to approximating the first order interacting space with only the leading subpace, which explains why the the sizes of the correlation energies are systematically underestimated. Similar behaviors are also observed for all other spin states (see SI-Figure S1), where the shapes of the potential energy curves visually resemble the reference method. This suggests that $\left(E^{\mathrm{MP2}}_{\mathrm{dressed}} - E^{\mathrm{eff}}_{S}\right)$ might be used as an efficient approximation that avoids the PCG iteration for solving E^{eff}_{T} in Table I, and more extensive benchmarks in future works are needed to conclude whether this

property is indeed generally true especially when large active space is used. Lastly, once the inter-site interactions are recovered through $\left(E^{\mathrm{MP2}}_{\mathrm{dressed}} - E^{\mathrm{eff}}_{S} + E^{\mathrm{eff}}_{T}\right)$, the resulting energies (blue dots) are in good agreement with the reference codes (smaller white dots). This again confirms that because supporting subspace factorization is analytically exact, it is capable of recovering strong inter-site interactions near the conical intersections.

In the supporting information, we have included similar test results on butadiene and uracil. The calculations on butadiene (SI-Figure S2) include 2 singlet states and 3 triplet states (active space (3e, 4o)), as well as 3 doublet states and 3 quartet states (active space (3e, 4o)), and the maximum difference in the absolute energies is 0.0053 eV (0.122 kcal/mol). The calculations on uracil (SI-Figure S3) include 3 singlet states and 2 triplet states (active space (6e, 6o)), as well as 4 doublet states (active space (5e, 6o)), and the maximum difference in the absolute energies is also around 0.0053 eV (0.122 kcal/mol). The good agreement in these tests shows that the spin-adapted supporting subspace formulation is capable of providing accurate XMS-CASPT2 energies for arbitrary spin states. Although the supporting subspace factorization is analytically exact based on the proof presented in Section II, numerical differences are expected to exist between TERACHEM and BAGEL due to that they use different approximations to two electron-repulsion integrals (ERIs): BAGEL uses density fitting (DF) approximated ERIs for both SA-CASSCF as well as XMS-CASPT2 calculations, while TERACHEM uses exact ERIs for SA-CASSCF calculations but uses tensor hyper-contraction (THC) approximated ERIs for XMS-CASPT2. The numerical errors in absolute energies observed in the above tests are well within chemical accuracy of 1kcal/mol, and are consistent with numerical errors reported in previous benchmark studies that compare THC-MP2 with DF-MP2.[41]

B. Performance

To test the performance of the spin-free supporting subspace XMS-CASPT2, we use butadiene (4 active orbitals) or hexatriene (6 active orbitals) solvated in increasing number of methanol molecules as the test systems, and study how the computational cost depends on the different choices of spin states, active space settings and number of atomic orbitals.

In the SS-SR contraction scheme of XMS-CASPT2, the computational cost is dominated

by solving the state-specific Bloch equation (Eq. 4) to evaluate the diagonal element (Eq.5) in the effective Hamiltonian, while the computational cost of the off-diagonal element (Eq.6) is almost negligible. As shown in SI-Figure S4, evaluating the off-diagonal elements is about 10x faster than the diagonal elements. Therefore, we will focus on analyzing the performance of the diagonal element in the following discussions. The spin-adapted double excitations (Eq.10 and Eq.11) treat different spin states in the same way. Thus it is expected that the computational cost stays almost the same regardless of the spin properties. As shown in Figure 3(a), the total computation time for singlet states and doublet states are almost identical, which is a major advantage over the spin orbital formulation from the original paper.

When comparing the total computational time of using 4 active orbitals versus 6 active orbitals, Figure 3(a) also shows that they are similar in scaling with respect to the number of atomic orbitals but differ in the prefactor. To understand this, the total computation time is further divided into computing the dressed MP2 energy and the remainder energy (including E_S^{eff} and E_T^{eff} , see Table I). In this work, THC-MP2 is used to calculate the dressed MP2 energy. The computational cost formally scales as $O(N^4)$ with respect to the number of dressed orbitals, which should primarily depends on the number of atomic orbitals while the active space size has very little effect. As shown in Figure 3(b), the red solid line (dressed MP2 energy with 4 active orbitals) and the red dashed line (dressed MP2 energy with 6 active orbitals) almost overlap, and the computational cost increases roughly as $O(N^{3.1})$ with the number of atomic orbitals for the systems tested. Calculating the remainder term requires Fock builds and preconditioned conjugate gradient. As discussed in Section II E, we expect the computational cost to formally scales as $O(N^3)$ with respect to the number of atomic orbitals, and increases as n_{act}^2 with increasing number of active orbitals. As shown in Figure 3(b), the blue solid line (remainder with 4 active orbitals) and the blue dashed line (remainder with 6 active orbitals) are similar in the scaling, i.e. around $O(N^{2.5})$ with the number of atomic orbitals for the systems tested. On the other hand, due to the difference in the active orbitals, the prefactor from using 6 active orbitals is larger than that of 4 active orbitals, by roughly $6^2/4^2 = 2.25$. When combining the two parts together, the dressed MP2 energy terms will eventually dominate for large systems due to its higher scaling. For the systems tested, since the remainder part still takes more time than the MP2 term, the

overall performance observed in Figure 3(a) resembles more the behavior of the remainder term. These results show that the supporting subspace factorization can effectively reduce the scaling of XMS-CASPT2 calculations as first demonstrated in the original paper for singlet states, and the spin-free formulation allows similar scaling reduction to be achieved for arbitrary spin states.

When comparing the spin-free formulation with the spin-orbital formulation in the original paper, in addition to being able to treat arbitrary spin states, the prefactor can be further reduced even for singlet states by taking advantage of the symmetry properties of the spin-adapted tensors. Figure 4 compares this work and the original paper for calculating singlet state energies. It is expected that there is no difference in the dressed MP2 energy between the new (red solid line) and old (red dashed line) implementations, since the corresponding computational cost only depends on the number of dressed orbitals. However, the symmetry of the supporting subspace tensors and the trailing subspace tensors can be used when calculating the remainder term. As a result, the remainder term using the new spin-free implementation (blue solid line) is faster than the old implementation (blue dashed line) by almost a factor of 2. This shows that the symmetry of tensors is another advantage of the spin-free formulation.

Both Figure 3 and Figure 4 focus on scaling reduction and prefactor reduction in terms of computation time. In addition, it is worth pointing out that with supporting subspace factorization, the dimension of linear system that needs to be explicitly solved are either in the supporting subspace (Eq.65) or in the trailing subspace (Eq.68). As a result, only the trailing subspace tensors and supporting subspace tensors need to be explicitly stored in memory, which only scales as $O(N^2)$ with the number of atomic orbitals and increases as n_{act}^2 with the number of active orbitals. In fact, for all calculations presented in this paper, all intermediate quantities can be stored using up to 48GB of memory, and no disk space is required as scratch space. Therefore, the spin-free supporting subspace factorization reduces the computational cost of XMS-CASPT2 calculations both in operations and memory, which allows calculations on large molecules to be carried out on standard desktop computers.

C. Application to photoreactions sensitive to magnetic field effects

The previous tests have shown that spin-free supporting subspace factorization can provide accurate XMS-CASPT2 energies for arbitrary spin states with reduced computational cost. As a demonstration, we apply the new method to the photoreaction between 10-methylphenothiazine (denoted as D in the following discussions) and nitroxide-linked acceptor(denoted as A-R). This photoreaction has been studied by Mori et.al experimentally,[71] who showed that the ratio between two reaction products, i.e.neutral product [D A-R] versus charged product [D+, A-R-], is subject to magnetic field effects.

Mori et.al proposed that the magnetic sensitivity of the reaction arises from that different spin states differ in the number of channels leading to each product, thus the relative population on each spin state will affect the product yield. To be more specific, light absorption first induces local excitation of D, and the total spin of of the local excitation state [D* A-R] can either be doublet and quartet, and both can lead to the neutral product. In addition, molecules can move from the local excitation states to charge transfer states [D+, A-R-] from either the doublet or the quartet states, leading to the charged product. Lastly, only molecules on the doublet charge transfer state can undergo backward charge transfer and relax to the doublet ground state (D0), leading to the neutral product. Although there are other states involved in the mechanisms proposed by Mori et.al, we will only focus on the aforementioned states in our calculations.

Based on the above mechanisms, we first use SA-CASSCF with polarizable continuum model (PCM)[72] to locate the MECI between the local excitation state and the charge transfer state, which exist both for doublet and quartet states. Four doublet states and two quartet states are included in the calculations. Dielectric constant of $\epsilon = 18.2$ is applied in PCM corresponding to the methanol solvent used in the experimental paper. In addition, SA-CASSCF/PCM is also used to locate the MECI between the charge transfer state with the ground state, which only exists for doublet states. We then calculate XMS-CASPT2 energies along the interpolation pathway that connects the two MECIs. The geometries of the two MECIs as well as the XMS-CASPT2 potential energy curves are presented in Figure 5. PCM effects are included into the zeroth-order Hamiltonian when calculating the XMS-CASPT2 energies.

By analyzing the characteristics of each excited state through attachment-detachment analysis[73](see SI-Figure S5), we found that the local excitation states [D* A-R] (D3, Q2) are higher in energy than the charge transfer states [D+, A-R-] (D1, D2, Q1) along the chosen pathway. Figure 5 also shows that at XMS-CASPT2 level, for both the local excitations and charge transfer excitations, the doublet and quartet states are energetically very close. As pointed out in Mori et.al,[71] such property is essential for notable magnetic effects as the energy difference will be highly senstive to the strength of the magnetic fields, allowing the relative population to be tuned correspondingly. In addition, our calculations also show that the potential energy curves are almost barrierless on the charge transfer state between the two MECIs. This may suggest that once a molecule populates the charge transfer state, molecules with doublet spin may quickly transfer to the ground state, while molecules with quartet spins will remain on the excited state. Such difference will further improve the yields of the neutral products from doublet states compared to the quartet states. In SI-Figure S6, we also compare the XMS-CASPT2 potential energy curves with SA-CASSCF along the same pathway, and notable differences can be observed. For example, at the D1/D0 MECI geometry, the energy gap between D2 and D4 from SA-CASSCF is much larger than that of XMS-CASPT2. For the local excitation states, potential energy curves from XMS-CASPT2 are relatively flat, while curves from SA-CASSCF are much steeper. This comparison shows that dynamic correlation effects are indispensable for accurate descriptions of excited state potential energy surfaces.

The active space (4e, 3o) used in the above calculations is certainly not sufficient to fully capture the static correlation in the long conjugation system of the studied molecules, and it is possible that the potential energy curves may change qualitatively when the active space is expanded. This limitation exists because our current implementation only supports small active spaces (up to 6 active electrons), and the calculations should be revisited when the method can be used with large active spaces, which will require more future work. At the same time, Figure 5 is the first test that applies supporting subspace factorization to a finely interpolated path for a system with close to a hundred atoms, and the results demonstrate that supporting subspace factorization is still able to produce smooth potential energy surfaces as the system gets large.

IV. CONCLUSIONS

In this paper, we derived supporting subspace factorization based on spin-free formulation, which enables scaling reduction of XMS-CASPT2 for arbitrary spins. Calculations on the test systems show that energies obtained from the XMS-CASPT2 using supporting subspace factorization agrees with conventional implementation to 0.01eV. In addition, the derivations presented in this work are based on the connections between supporting subspace factorization with Kronecker sum and Löwdin partition, which reveals its physical interpretation that is not obvious in the original paper. From the results and discussion in Section III, we have also identified a few places that need improvements through future works, in particular possible ways to go beyond real level shifting and enable large active space calculations.

In the example studies shown in Figure 5, the geometries at Franck-Condon point and MECI are optimized at SA-CASSCF level. Since notable differences have been observed between SA-CASSCF and XMS-CASPT2 potential energy curves, more rigorous studies require optimizing these geometries using XMS-CASPT2 instead. This requires developing the corresponding analytical gradients for XMS-CASPT2 with the spin-free supporting subspace factorization applied. Previously, we have already developed the analytical gradients for state specific CASPT2 using supporting subspace factorization in the spin-orbital formulation.[53] The main computational bottleneck of CASPT2 gradient is solving the "lambda equation"[28] that provides the lagrange multipliers corresponding to the double excitation amplitudes. Because the lambda equation takes similar form as the Bloch equation, the supporting subspace factorization has been shown to be effective in reducing the computational cost of singlet state gradients, and this idea can be naturally generalized to spin-free formulation for arbitrary spin states. In addition, solving the state-specific lambda equation is a major step towards evaluating the analytical gradients and non-adiabatic coupling vectors for XMS-CASPT2.[28,29] Therefore, to allow efficient critical point searches and nonadiabatic molecular dynamics simulations at XMS-CASPT2 level, applying spin-free supporting subspace factorization to analytical gradients and NAC calculations will become important future directions.

In addition to analytical gradients and non-adiabatic couplings, studies of photochemistry also require other properties, most importantly the transition dipole moment and spin-orbit

couplings. Therefore, it is necessary to study how these quantities can be computed when the XMS-CASPT2 wavefunction is in the supporting subspace factorized form. The transition dipole moment[74] involves only one-electron operator, and requires the one-particle transition density matrix of XMS-CASPT2. The spin-orbit coupling is more complicated as the Pauli-Breit operator includes both one-electron and two-electron contributions.[75,76] As an intial step, one can neglect the two electron contribution and correct the one-electron operator using effective nuclear charges.[77] Under such approximation, one only needs to build one-particle density matrix between two states of different spins. At the moment, because the SA-CASSCF codes we use only solve for wavefunctions with $S_z = 0$, the corresponding supporting subspace factorized XMS-CASPT2 wavefunctions are limited to $S_z = 0$. Computing spin orbit couplings especially in the x and y directions will likely require studying how the angular momentum lowering and raising operators can be applied to wavefunction in the factorized form such that the corresponding density matrix can be calculated.

SUPPLEMENTARY MATERIAL

See supplementary material for detailed mathematical derivations, additional test results, as well as sample input and output files from this work.

AUTHOR DECLARATION

The author has no conflicts to disclose.

DATA AVAILABILITY

For each system studied in this work, one sample calculation that includes input and output files is provided in the supplementary information. Additional data is available from the corresponding author upon reasonable request.

ACKNOWLEDGEMENTS

This work was supported by the startup funds of the UC Davis Department of Chemistry.

TABLE I. Algorithms of XMS-CASPT2 calculations using supporting subspace factorization. For each step, equation number in the main text as well as SI-section number that describes the computational details are both listed.

	Algorithm	**Equation**	**SI-Section**
	I. Solve state-specific CASPT2 for each state		
	MP2 energy in dressed orbitals		
1	Build hole coupling matrix $\gamma_{hh'}$	17	1.1
2	Build particle coupling matrix $\bar{\gamma}_{pp'}$	18	1.1
3	Diagonalize $\gamma_{hh'}$ to get dressed hole ω_η	25	
4	Diagonalize $\bar{\gamma}_{pp'}$ to get dressed particle $\bar{\omega}_\pi$	26	
5	Call MP2 to compute $E_{\mathrm{MP2}}^{\mathrm{dressed}}$	33	
	Remove supporting subspace contribution		
6	Calculate $Q_S^{(+)}\mathbf{t}_{\mathrm{apx}}$ and $Q_S^{(-)}\mathbf{t}_{\mathrm{apx}}$	64	1.3.3
7	Solve support tensors $\mathbf{s}_{\mathrm{apx}}^{(+)}$ and $\mathbf{s}_{\mathrm{apx}}^{(-)}$	65	1.3.4
8	Compute $E_S^{\mathrm{eff}} = \left(Q_S\mathbf{t}_{\mathrm{apx}}\right)^T \cdot \mathbf{s}_{\mathrm{apx}}$	63	
	Add trailing subspace contribution		
9	Calculate $Q_T\mathbf{h}^{\mathrm{eff}}$	72	1.3.5
10	Solve $Q_T\mathbf{t}$ from linear equation using PCG	68	1.3.6
	Update trial vector $\mathbf{v}_{\mathrm{trial}}$		
	Solve support tensors $\mathbf{s}_{\mathrm{trial}}^{(+)}$ and $\mathbf{s}_{\mathrm{trial}}^{(-)}$	73	
	Calculate matrix vector product	74	
	Loop until converged		
11	Compute $E_T^{\mathrm{eff}} = -\left(Q_T\mathbf{h}^{\mathrm{eff}}\right)^T \cdot \left(Q_T\mathbf{t}\right)$	66	
12	$E_{\mathrm{CASPT2}} = E_{\mathrm{MP2}}^{\mathrm{dressed}} - E_S^{\mathrm{eff}} + E_T^{\mathrm{eff}}$	60	
	Level shift correction		
13	Solve $\mathbf{s}_t^{(+)}$ and $\mathbf{s}_t^{(-)}$ for $P_L\mathbf{t}$ in factorized form	76	
14	Compute $\Delta E_{\mathrm{shift}}$ and add to E_{CASPT2}		
	II. Solve XMS-CASPT2 energies		
15	Add E_{CASPT2} to diagonal element H_{II}^{eff}	5	
16	Compute off-diagonal elements H_{IJ}^{eff}	6	
17	Diagonalize H^{eff} for XMS-CASPT2 energies		

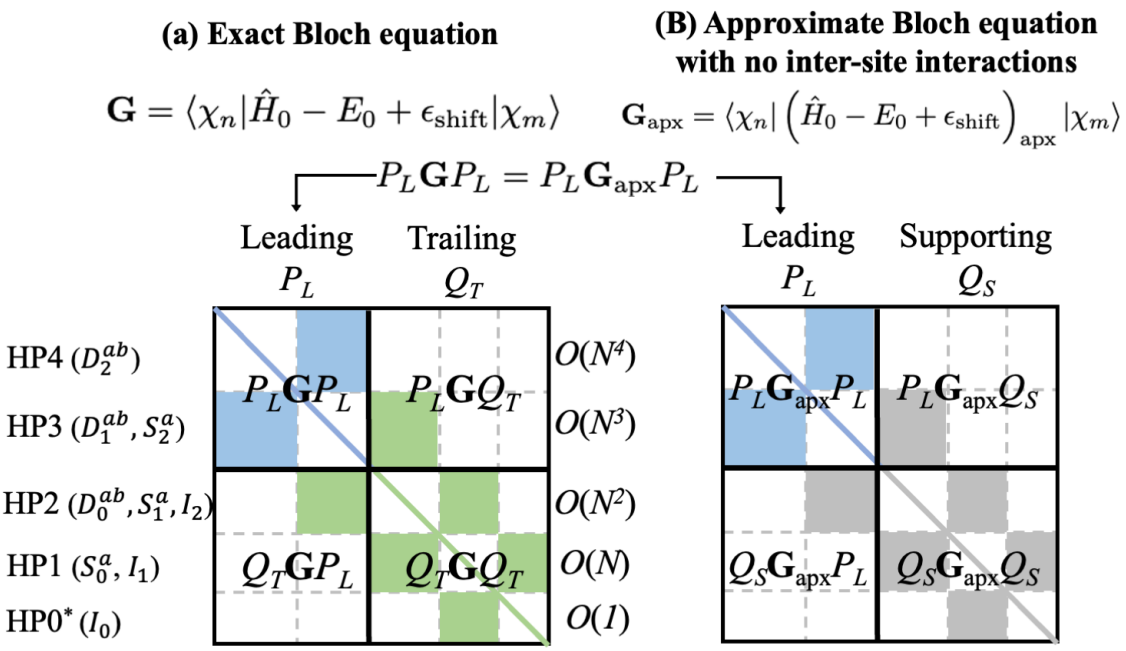

FIG. 1. Illustration of partitioning the exact Bloch equation $\mathbf{G}$ into the leading subspace (P_L) and trailing subspace (Q_T), and partitioning the approximate Bloch equation in the absence of inter-site interactions $\mathbf{G}_b$ into the leading subspace (P_L) and supporting subspace (Q_S). The two matrices are identical in the leading subspace, as shown by the equation $P_L\mathbf{G}P_L = P_L\mathbf{G}_{\text{apx}}P_L$. Partition of space in this work depends on both the number of holes in closed orbitals and the number of electrons in virtual orbitals. "HPn" denotes the type of double excitations that have n out of 4 indices to be either closed or virtual orbitals. The symbols in the parenthesis show the correspondence with the internal (I), semi-internal (S^a) and external (D^{ab}) partition commonly used in standard CASPT2 studies. Given an active space settings, the number of excitations in "HPn" group increases as $O(N^n)$ with the number of atomic orbitals in the system. "HP0*" indicates that such excitations are not included when the reference is of complete active space (CAS), but should be considered if the reference is of restricted active space (RAS).

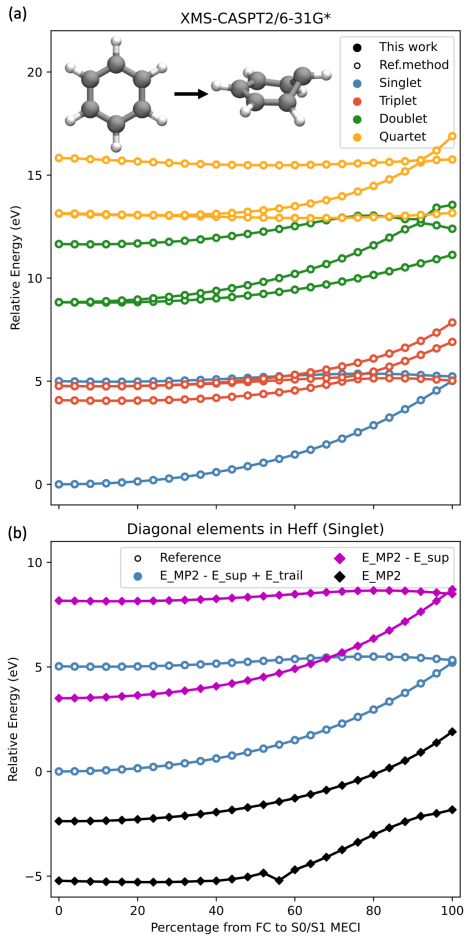

FIG. 2. (a) Potential energy curves for benzene along the pathway from Franck-Condon point (FC) to the S0/S1 MECI. Supporting subspace XMS-CASPT2 results (this work) are shown in solid colored dots, and conventional XMS-CASPT2 results (Ref. method, using BAGEL) were shown in white dots. Energies from TERACHEM and BAGEL are shifted by the same constant, i.e. subtracting S0 energy at first image computed by BAGEL. The calculations include 2 singlets states (blue) and 3 triplet states (red) computed with XMS-CASPT2(4e,4o)/6-31G*, as well as 3 doublet states (green) and 3 quartet states (orange) computed with XMS-CASPT2(3e,4o)/6-31G*. The coordinates as well as sample input and output files are provided in the zip file of the supplementary material. Maximum difference in the absolute energies between the two methods is 0.0177 eV (0.408 kcal/mol). (b) Changes of potential energy curves when the correlation energies are computed as $E^{\mathrm{MP2}}_{\mathrm{dressed}}$ (black diamonds), $\left(E^{\mathrm{MP2}}_{\mathrm{dressed}} - E^{\mathrm{eff}}_{S}\right)$ (magenta diamonds), $\left(E^{\mathrm{MP2}}_{\mathrm{dressed}} - E^{\mathrm{eff}}_{S} + E^{\mathrm{eff}}_{T}\right)$ (blue dots) and reference method (white dots) respectively. Energies correspond to state-specific CASPT2 potential energies for singlet states, i.e. diagonal elements in the $\mathbf{H}^{\mathrm{eff}}$ in Eq.5 without level shift correction.

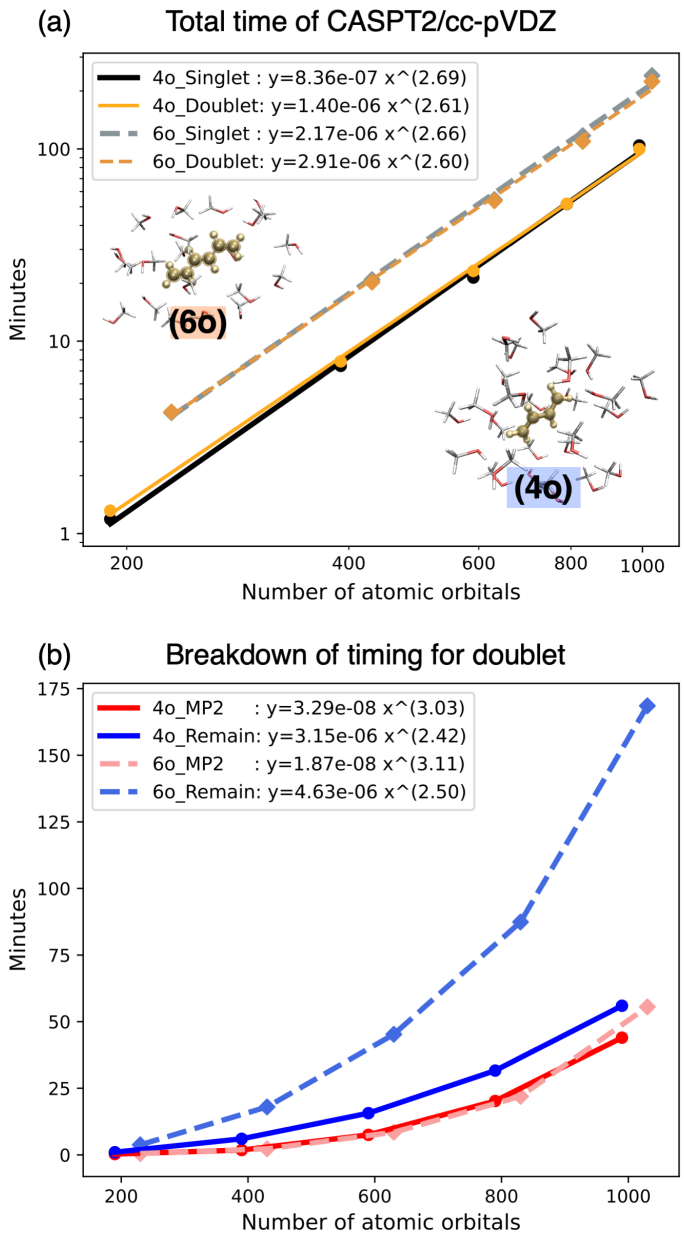

FIG. 3. Performance of spin-free supporting subspace CASPT2/cc-pVDZ. The upper inset geometry illustrates hexatriene solvated with increasing number of methanol molecules, and are computed with (6e,6o) for singlet states and (5e, 6o) for doublet states. The lower inset geometry illustrates solvated butadiene, and are computed with (4e,4o) or (3e, 4o) for singlet and doublet states respectively. (a) shows the the total timing in logarithm scale. (b) shows the breakdown of timing into dressed MP2 energy and the remainder term in linear scale. Both (a) and (b) include computational scaling obtained from power-law fitting using scipy. All timings were performed with using one NVIDIA GeForce GTX 1080 Ti GPUs and Intel Xeon E5-2643 CPUs.

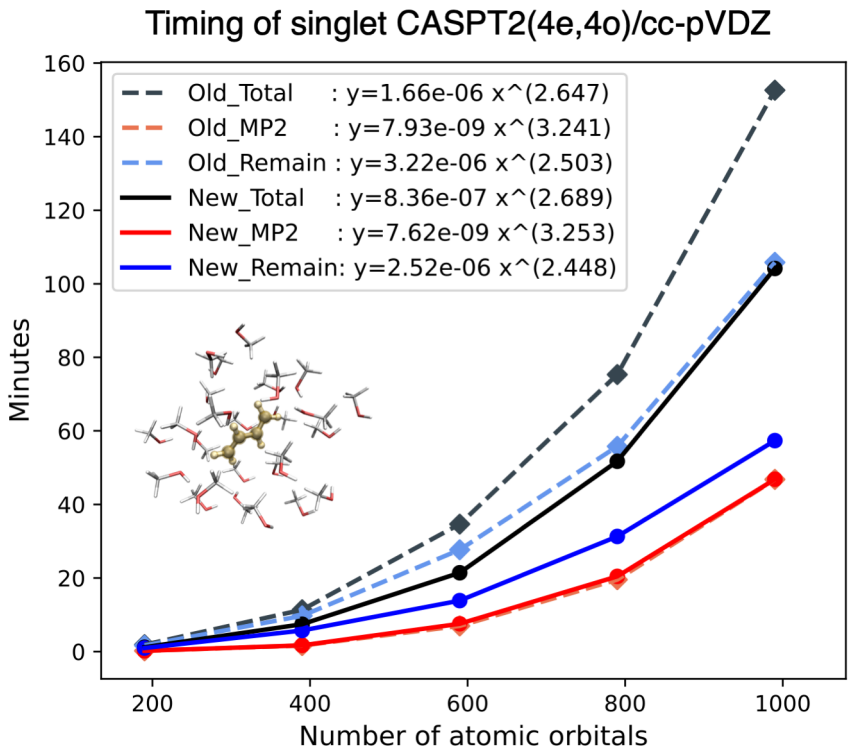

FIG. 4. Performance comparison of supporting subspace CASPT2 for singlet states between using the original spin orbital formulation ("old") and the new spin-free formulation (this work, "new"). The solvated butadienes from Figure 3 are used as the test systems. Computational scalings are obtained from power-law fitting using scipy.

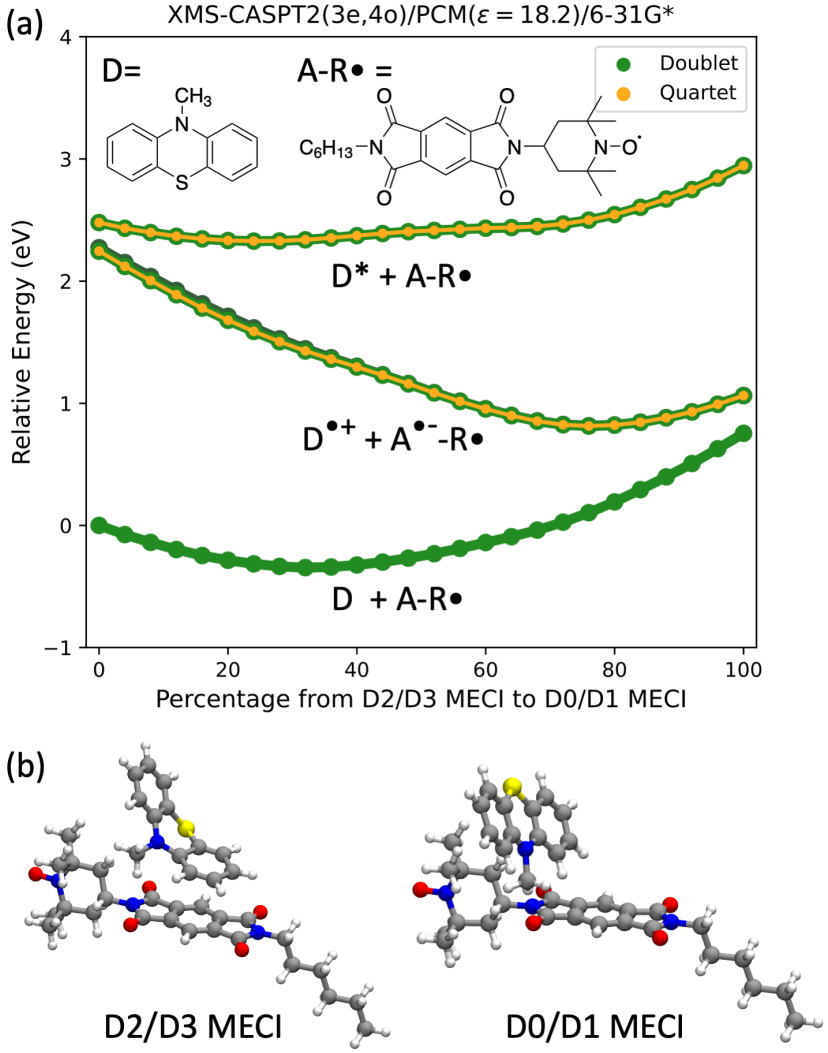

FIG. 5. The XMS-CASPT2 energies of the photoreaction between 10-methylphenothiazine (see inset structure "D") and nitroxide-linked acceptor (see inset structure "A-R"). (a) Potential energy curves of the four doublet states (green) and two quartet states (yellow). Note that D1 and D2 are energetically almost degenerate and are both of character [D+, A-R-], thus D2 energies are colored with a darker green and are drawn behind the D1 dots. Relative energies are shown with respect to the D0 energy of the first structure. The geometries are generated from an interpolation path connecting the SA-CASSCF-optimized D2/D3 MECI and D0/D1 MECI. The characteristics of each state is determined from attachment-detachment analysis (see SI-Figure S5). (b) Geometries of D2/D3 MECI and D0/D1 MECI respectively. These calculations were performed using two NVIDIA GeForce GTX 1080 Ti GPUs. 48GB memory is used for storing intermediate variables, and disk space is not needed as scratch space for temporary variables.

REFERENCES

[1]J. H. Correia, J. A. Rodrigues, S. Pimenta, T. Dong, and Z. Yang, "Photodynamic Therapy Review: Principles, Photosensitizers, Applications, and Future Directions," Pharmaceutics **13**, 1332 (2021).

[2]T. C. Pham, V.-N. Nguyen, Y. Choi, S. Lee, and J. Yoon, "Recent Strategies to Develop Innovative Photosensitizers for Enhanced Photodynamic Therapy," Chemical Reviews **121**, 13454–13619 (2021).

[3]W. J. Glover, T. Mori, M. S. Schuurman, A. E. Boguslavskiy, O. Schalk, A. Stolow, and T. J. Martínez, "Excited state non-adiabatic dynamics of the smallest polyene, trans 1,3-butadiene. II. Ab initio multiple spawning simulations," The Journal of Chemical Physics **148**, 164303 (2018).

[4]C. Melania Oana and A. I. Krylov, "Dyson orbitals for ionization from the ground and electronically excited states within equation-of-motion coupled-cluster formalism: Theory, implementation, and examples," The Journal of Chemical Physics **127**, 234106 (2007).

[5]N. J. Turro, *Modern Molecular Photochemistry* (University Science Books, 1991).

[6]C. T. Rodgers and P. J. Hore, "Chemical magnetoreception in birds: The radical pair mechanism," Proceedings of the National Academy of Sciences **106**, 353–360 (2009).

[7]R. Wiltschko, C. Nießner, and W. Wiltschko, "The Magnetic Compass of Birds: The Role of Cryptochrome," Frontiers in Physiology **12** (2021).

[8]S. Battaglia, I. Fdez. Galván, and R. Lindh, "Chapter 5 - Multiconfigurational quantum chemistry: The CASPT2 method," in *Theoretical and Computational Photochemistry*, edited by C. García-Iriepa and M. Marazzi (Elsevier, 2023) pp. 135–162.

[9]P. Pulay, "A perspective on the CASPT2 method," International Journal of Quantum Chemistry **111**, 3273–3279 (2011).

[10]B. O. Roos, P. R. Taylor, and P. E. M. Sigbahn, "A complete active space SCF method (CASSCF) using a density matrix formulated super-CI approach," Chemical Physics **48**, 157–173 (1980).

[11]B. O. Roos, "The complete active space SCF method in a fock-matrix-based super-CI formulation," International Journal of Quantum Chemistry **18**, 175–189 (1980).

[12]M. W. Schmidt and M. S. Gordon, "The Construction and Interpretation of Mcscf Wavefunctions," Annual Review of Physical Chemistry **49**, 233–266 (1998).

[13]I. Shavitt and R. J. Bartlett, *Many-Body Methods in Chemistry and Physics: MBPT and Coupled-Cluster Theory* (Cambridge University Press, 2009).

[14]B. O. Roos, P. Linse, P. E. M. Siegbahn, and M. R. A. Blomberg, "A simple method for the evaluation of the second-order-perturbation energy from external double-excitations with a CASSCF reference wavefunction," Chemical Physics **66**, 197–207 (1982).

[15]Kerstin. Andersson, P. A. Malmqvist, B. O. Roos, A. J. Sadlej, and Krzysztof. Wolinski, "Second-order perturbation theory with a CASSCF reference function," The Journal of Physical Chemistry **94**, 5483–5488 (1990).

[16]K. Andersson, P.-Å. Malmqvist, and B. O. Roos, "Second-order perturbation theory with a complete active space self-consistent field reference function," The Journal of Chemical Physics **96**, 1218–1226 (1992).

[17]B. O. Roos and K. Andersson, "Multiconfigurational perturbation theory with level shift — the Cr2 potential revisited," Chemical Physics Letters **245**, 215–223 (1995).

[18]G. Ghigo, B. O. Roos, and P.-Å. Malmqvist, "A modified definition of the zeroth-order Hamiltonian in multiconfigurational perturbation theory (CASPT2)," Chemical Physics Letters **396**, 142–149 (2004).

[19]S. Battaglia, L. Fransén, I. Fdez. Galván, and R. Lindh, "Regularized CASPT2: An Intruder-State-Free Approach," Journal of Chemical Theory and Computation **18**, 4814–4825 (2022).

[20]K. Andersson and B. O. Roos, "Multiconfigurational second-order perturbation theory: A test of geometries and binding energies," International Journal of Quantum Chemistry **45**, 591–607 (1993).

[21]K. G. Dyall, "The choice of a zeroth-order Hamiltonian for second-order perturbation theory with a complete active space self-consistent-field reference function," The Journal of Chemical Physics **102**, 4909–4918 (1995).

[22]C. Kollmar, K. Sivalingam, and F. Neese, "An alternative choice of the zeroth-order Hamiltonian in CASPT2 theory," The Journal of Chemical Physics **152**, 214110 (2020).

[23]K. Andersson, "Different forms of the zeroth-order Hamiltonian in second-order perturbation theory with a complete active space self-consistent field reference function," Theoretica

chimica acta **91**, 31–46 (1995).

[24]J. Finley, P.-Å. Malmqvist, B. O. Roos, and L. Serrano-Andrés, "The multi-state CASPT2 method," Chemical Physics Letters **288**, 299–306 (1998).

[25]T. Shiozaki, W. Győrffy, P. Celani, and H.-J. Werner, "Communication: Extended multi-state complete active space second-order perturbation theory: Energy and nuclear gradients," The Journal of Chemical Physics **135**, 081106 (2011).

[26]S. Battaglia and R. Lindh, "Extended Dynamically Weighted CASPT2: The Best of Two Worlds," Journal of Chemical Theory and Computation **16**, 1555–1567 (2020).

[27]P. Celani and H.-J. Werner, "Analytical energy gradients for internally contracted second-order multireference perturbation theory," The Journal of Chemical Physics **119**, 5044–5057 (2003).

[28]B. Vlaisavljevich and T. Shiozaki, "Nuclear Energy Gradients for Internally Contracted Complete Active Space Second-Order Perturbation Theory: Multistate Extensions," Journal of Chemical Theory and Computation **12**, 3781–3787 (2016).

[29]J. W. Park and T. Shiozaki, "Analytical Derivative Coupling for Multistate CASPT2 Theory," Journal of Chemical Theory and Computation **13**, 2561–2570 (2017).

[30]M. Feyereisen, G. Fitzgerald, and A. Komornicki, "Use of approximate integrals in ab initio theory. An application in MP2 energy calculations," Chemical Physics Letters **208**, 359–363 (1993).

[31]F. Weigend, M. Häser, H. Patzelt, and R. Ahlrichs, "RI-MP2: Optimized auxiliary basis sets and demonstration of efficiency," Chemical Physics Letters **294**, 143–152 (1998).

[32]O. Vahtras, J. Almlöf, and M. W. Feyereisen, "Integral approximations for LCAO-SCF calculations," Chemical Physics Letters **213**, 514–518 (1993).

[33]R. A. Friesner, "Solution of self-consistent field electronic structure equations by a pseudospectral method," Chemical Physics Letters **116**, 39–43 (1985).

[34]T. J. Martinez and E. A. Carter, "Pseudospectral Mo/ller–Plesset perturbation theory through third order," The Journal of Chemical Physics **100**, 3631–3638 (1994).

[35]M. N. Ringnalda, M. Belhadj, and R. A. Friesner, "Pseudospectral Hartree–Fock theory: Applications and algorithmic improvements," The Journal of Chemical Physics **93**, 3397–3407 (1990).

[36]F. Aquilante, L. Gagliardi, T. B. Pedersen, and R. Lindh, "Atomic Cholesky decompositions: A route to unbiased auxiliary basis sets for density fitting approximation with tunable accuracy and efficiency," The Journal of Chemical Physics **130**, 154107 (2009).

[37]F. Aquilante, T. B. Pedersen, and R. Lindh, "Low-cost evaluation of the exchange Fock matrix from Cholesky and density fitting representations of the electron repulsion integrals," The Journal of Chemical Physics **126**, 194106 (2007).

[38]H. Koch, A. Sánchez de Merás, and T. B. Pedersen, "Reduced scaling in electronic structure calculations using Cholesky decompositions," The Journal of Chemical Physics **118**, 9481–9484 (2003).

[39]E. G. Hohenstein, R. M. Parrish, and T. J. Martínez, "Tensor hypercontraction density fitting. I. Quartic scaling second- and third-order Møller-Plesset perturbation theory," The Journal of Chemical Physics **137**, 044103 (2012).

[40]R. M. Parrish, E. G. Hohenstein, T. J. Martínez, and C. D. Sherrill, "Tensor hypercontraction. II. Least-squares renormalization," The Journal of Chemical Physics **137**, 224106 (2012).

[41]C. Song and T. J. Martínez, "Atomic orbital-based SOS-MP2 with tensor hypercontraction. I. GPU-based tensor construction and exploiting sparsity," The Journal of Chemical Physics **144**, 174111 (2016).

[42]J. Almlöf, "Elimination of energy denominators in Møller—Plesset perturbation theory by a Laplace transform approach," Chemical Physics Letters **181**, 319–320 (1991).

[43]M. Häser and J. Almlöf, "Laplace transform techniques in Mo/ller–Plesset perturbation theory," The Journal of Chemical Physics **96**, 489–494 (1992).

[44]C. Song and T. J. Martínez, "Analytical gradients for tensor hyper-contracted MP2 and SOS-MP2 on graphical processing units," The Journal of Chemical Physics **147**, 161723 (2017).

[45]J. I. Cirac, D. Pérez-García, N. Schuch, and F. Verstraete, "Matrix product states and projected entangled pair states: Concepts, symmetries, theorems," Reviews of Modern Physics **93**, 045003 (2021).

[46]R. Orús, "A practical introduction to tensor networks: Matrix product states and projected entangled pair states," Annals of Physics **349**, 117–158 (2014).

[47]G. K.-L. Chan, A. Keselman, N. Nakatani, Z. Li, and S. R. White, "Matrix product operators, matrix product states, and ab initio density matrix renormalization group algorithms," The Journal of Chemical Physics **145**, 014102 (2016).

[48]U. Schollwöck, "The density-matrix renormalization group in the age of matrix product states," Annals of Physics January 2011 Special Issue, **326**, 96–192 (2011).

[49]E. G. Hohenstein, B. S. Fales, R. M. Parrish, and T. J. Martínez, "Rank-reduced coupled-cluster. III. Tensor hypercontraction of the doubles amplitudes," The Journal of Chemical Physics **156**, 054102 (2022).

[50]R. Schutski, J. Zhao, T. M. Henderson, and G. E. Scuseria, "Tensor-structured coupled cluster theory," The Journal of Chemical Physics **147**, 184113 (2017).

[51]C. Song and T. J. Martínez, "Reduced scaling CASPT2 using supporting subspaces and tensor hyper-contraction," The Journal of Chemical Physics **149**, 044108 (2018).

[52]C. Song and T. J. Martínez, "Reduced scaling extended multi-state CASPT2 (XMS-CASPT2) using supporting subspaces and tensor hyper-contraction," The Journal of Chemical Physics **152**, 234113 (2020).

[53]C. Song, J. B. Neaton, and T. J. Martínez, "Reduced scaling formulation of CASPT2 analytical gradients using the supporting subspace method," The Journal of Chemical Physics **154**, 014103 (2021).

[54]W. Kutzelnigg and D. Mukherjee, "Irreducible Brillouin conditions and contracted Schrödinger equations for n-electron systems. II. Spin-free formulation," The Journal of Chemical Physics **116**, 4787–4801 (2002).

[55]C. Li and F. A. Evangelista, "Spin-free formulation of the multireference driven similarity renormalization group: A benchmark study of first-row diatomic molecules and spin-crossover energetics," The Journal of Chemical Physics **155**, 114111 (2021).

[56]D. Datta, L. Kong, and M. Nooijen, "A state-specific partially internally contracted multireference coupled cluster approach," The Journal of Chemical Physics **134**, 214116 (2011).

[57]T. Helgaker, P. Jorgensen, and J. Olsen, *Molecular Electronic-Structure Theory* (John Wiley & Sons, 2014).

[58]H. Nakano, "Quasidegenerate perturbation theory with multiconfigurational self-consistent-field reference functions," The Journal of Chemical Physics **99**, 7983–7992 (1993).

[59]A. J. Laub, *Matrix Analysis for Scientists and Engineers* (SIAM, 2005).

[60]K. Jacobs, *Quantum Measurement Theory and Its Applications* (Cambridge University Press, 2014).

[61]J. W. Park, R. Al-Saadon, N. E. Strand, and T. Shiozaki, "Imaginary Shift in CASPT2 Nuclear Gradient and Derivative Coupling Theory," Journal of Chemical Theory and Computation **15**, 4088–4098 (2019).

[62]N. Forsberg and P.-Å. Malmqvist, "Multiconfiguration perturbation theory with imaginary level shift," Chemical Physics Letters **274**, 196–204 (1997).

[63]A. Y. Sokolov and G. K.-L. Chan, "A transformed framework for dynamic correlation in multireference problems," The Journal of Chemical Physics **142**, 124107 (2015).

[64]F. A. Evangelista, "A driven similarity renormalization group approach to quantum many-body problems," The Journal of Chemical Physics **141**, 054109 (2014).

[65]P.-O. Löwdin, "Partitioning technique, perturbation theory, and rational approximations," International Journal of Quantum Chemistry **21**, 69–92 (1982).

[66]P. Celani and H.-J. Werner, "Multireference perturbation theory for large restricted and selected active space reference wave functions," The Journal of Chemical Physics **112**, 5546–5557 (2000).

[67]H.-J. WERNER, "Third-order multireference perturbation theory The CASPT3 method," Molecular Physics **89**, 645–661 (1996).

[68]S. Seritan, C. Bannwarth, B. S. Fales, E. G. Hohenstein, S. I. L. Kokkila-Schumacher, N. Luehr, J. W. Snyder, Jr., C. Song, A. V. Titov, I. S. Ufimtsev, and T. J. Martínez, "TeraChem: Accelerating electronic structure and ab initio molecular dynamics with graphical processing units," The Journal of Chemical Physics **152**, 224110 (2020).

[69]S. Seritan, C. Bannwarth, B. S. Fales, E. G. Hohenstein, C. M. Isborn, S. I. L. Kokkila-Schumacher, X. Li, F. Liu, N. Luehr, J. W. Snyder, C. Song, A. V. Titov, I. S. Ufimtsev, L.-P. Wang, and T. J. Martínez, "TeraChem: A graphical processing unit-accelerated electronic structure package for large-scale ab initio molecular dynamics," Wiley Interdisciplinary Reviews: Computational Molecular Science **11**, e1494 (2021).

[70]L.-P. Wang and C. Song, "Geometry optimization made simple with translation and rotation coordinates," The Journal of Chemical Physics **144**, 214108 (2016).

[71]Y. Mori, Y. Sakaguchi, and H. Hayashi, "Magnetic Field Effects on Chemical Reactions of Biradical Radical Ion Pairs in Homogeneous Fluid Solvents," The Journal of Physical

Chemistry A **104**, 4896–4905 (2000).

[72]C. Song, "State-averaged CASSCF with polarizable continuum model for studying photoreactions in solvents: Energies, analytical nuclear gradients, and non-adiabatic couplings," The Journal of Chemical Physics **156**, 104102 (2022).

[73]M. Head-Gordon, A. M. Grana, D. Maurice, and C. A. White, "Analysis of Electronic Transitions as the Difference of Electron Attachment and Detachment Densities," The Journal of Physical Chemistry **99**, 14261–14270 (1995).

[74]D. Robinson, "Comparison of the Transition Dipole Moments Calculated by TDDFT with High Level Wave Function Theory," Journal of Chemical Theory and Computation **14**, 5303–5309 (2018).

[75]D. G. Fedorov, S. Koseki, M. W. Schmidt, and M. S. Gordon, "Spin-orbit coupling in molecules: Chemistry beyond the adiabatic approximation," International Reviews in Physical Chemistry **22**, 551–592 (2003).

[76]C. M. Marian, "Spin-Orbit Coupling in Molecules," in *Reviews in Computational Chemistry* (John Wiley & Sons, Ltd, 2001) Chap. 3, pp. 99–204.

[77]S. Koseki, M. S. Gordon, M. W. Schmidt, and N. Matsunaga, "Main Group Effective Nuclear Charges for Spin-Orbit Calculations," The Journal of Physical Chemistry **99**, 12764–12772 (1995).